Journal of Medicinal Chemistry

Article

Discovery of (E)-N1-(3-fluorophenyl)-N3-(3-(2-(pyridin-2-yl)vinyl)-1H-indazol-6-yl)malonamide (CHMFL-KIT-033) as a Novel c-KIT T670I Mutant Selective Kinase Inhibitor for Gastrointestinal Stromal Tumors (GISTs)

Xuesong Liu, Beilei Wang, Cheng Chen, Ziping Qi, Fengming Zou, Junjie Wang, Chen Hu, Aoli Wang, Juan Ge, Qingwang Liu, Kailin Yu, Zhenquan Hu, Zongru Jiang, Wei Wang, Li Wang, Wenchao Wang, Tao Ren, Mingfeng Bai, Qingsong Liu, and Jing Liu

J. Med. Chem., **Just Accepted Manuscript** • DOI: 10.1021/acs.jmedchem.9b00176 • Publication Date (Web): 02 May 2019

Just Accepted

ACS Publications

is published by the American Chemical Society. 1155 Sixteenth Street N.W., Washington, DC 20036

Discovery of (*E*)-*N*1-(3-fluorophenyl)-*N*3-(3-(2-(pyridin-2-yl)vinyl)-1*H*-indazol-6-yl)malonamide (CHMFL-KIT-033) as a Novel c-KIT T670I Mutant Selective Kinase Inhibitor for Gastrointestinal Stromal Tumors (GISTs)

Xuesong Liu[1,2,8], Beilei Wang[1,2,8], Cheng Chen[1,2,8], Ziping Qi[1,3,8], Fengming Zou[1,3], Junjie Wang[1,2], Chen Hu[1,3], Aoli Wang[1,3,4], Juan Ge[1,2], Qingwang Liu[3,4], Kailin Yu[1,3], Zhenquan Hu[1,3], Zongru Jiang[1,2], Wei Wang[1,3,4], Li Wang[1,2], Wenchao Wang[1,2,3,4], Tao Ren[3,4,5], Mingfeng Bai[6], Qingsong Liu[1,2,3,4,7], Jing Liu[1,2,3,4*]*

1. High Magnetic Field Laboratory, Key Laboratory of High Magnetic Field and Ion Beam Physical Biology, Hefei Institutes of Physical Science, Chinese Academy of Sciences, Hefei, Anhui, 230031, China
2. University of Science and Technology of China, Hefei, Anhui, 230026, P. R. China
3. Precision Medicine Research Laboratory of Anhui Province, Hefei, Anhui, 230088, P. R. China
4. Precision Targeted Therapy Discovery Center, Institute of Technology Innovation, Hefei Institutes of Physical Science, Chinese Academy of Sciences, Hefei, Anhui, 230088, P. R. China
5. Precedo Pharmaceuticals Inc, Hefei, Anhui, 230088, P. R. China

6. Molecular Imaging Laboratory, Department of Radiology, University of Pittsburgh Cancer Institute, University of Pittsburgh, Pittsburgh, Pennsylvania 15219, United States
7. Institutes of Physical Science and Information Technology, Anhui University, Hefei, Anhui, 230601, P. R. China
8. These authors contribute equally

ABSTRACT

Gain-of-function mutations of c-KIT kinase play crucial pathological roles for the GISTs. Despite of the success of imatinib as the first line treatment of GISTs, dozens of drug-acquired resistant mutations emerge and c-KIT T670I is one of the most common mutants among them. Although several kinase inhibitors are capable of overcoming the T670I mutant, none of them can achieve the selectivity over the c-KIT wt which also plays important roles in a variety of physiological functions such as hematopoiesis. Starting from axitinib, through fragment hybrid type II kinase inhibitor design approach, we have discovered a novel inhibitor **24**, which not only exhibits potent activity to c-KIT T670I mutant but also achieves 12-fold selectivity over c-KIT wt. Compound **24** displays good antiproliferative effects against c-KIT T670I mutant driven GISTs cell lines (GIST-T1/T670I and GIST-5R), and also exhibits suitable in vivo PK profiles as well as dose-dependent antitumor efficacy. This study provides a proof-of-concept for developing c-KIT mutant selective inhibitor which theoretically can render better therapeutic window.

INTRODUCTION

Gastrointestinal stromal tumors (GISTs) are the most common mesenchymal neoplasm in the gastrointestinal tract. The overall incidence of GISTs ranges between 6.5 and 14.5 per million

each year in Europe and America.[1] Approximately 95% of GISTs express c-KIT, and the majority of them harbor activating mutations of c-KIT which play a critical pathogenic role in the development of GISTs.[2,3] c-KIT kinase belongs to type III receptor tyrosine kinase family which also includes FLT3, PDGFRs and CSF1R. Upon activation, c-KIT is involved in cell survival, migration and proliferation depending on the cell type[4]. Early hematopoietic cells[5,6], maturation cells such as mast cells, dendritic cells[7] and fully differentiated cells[8] are also dependent on c-KIT for proliferation, survival and normal functions. In addition, c-KIT actively triggers cell death in a variety of cancer cell lines except when engaged by its ligand stem cell factor (SCF). c-KIT acts both as a proto-oncogene via its kinase activity and as a tumor suppressor via its dependence receptor activity.[9] Gain-of-function mutations of c-KIT drive the pathology of several diseases especially the GITSs, therefore there have been extensive drug discovery efforts targeting this kinase.[10]

Imatinib (**1**) was approved as the first-line therapy for advanced GISTs (Figure 1). However, about 14% of the patients were insensitive to compound **1** initially,[11,12] and more than a half of responding patients developed drug resistance due to the acquisition of secondary mutations in kinase domain such as T670I within 2 years treatment[13-15]. Sunitinib (**2**)[16] and regorafenib (**3**)[17] were approved as the second and third line therapy respectively for GISTs to overcome some imatinib-resistant mutants, including the T670I mutant (Figure 1). However, due to their very low overall response rates and toxicities, the clinical application was limited. In addition, ponatinib (**4**)[18] and cabozantinib (**5**)[19] were also reported to be capable of overcoming the T670I mutant induced resistance (Figure 1). Axitinib (**6**)[20], an approved drug for renal cell carcinoma (RCC), is an orally available multitarget kinase inhibitor that potently inhibits c-KIT, PDGFRα/β and VEGFR1/2/3 (Figure 1). The kinase profiling data also revealed that it has strong binding

affinity to c-KIT (binding Kd: 3.7 nM) and c-KIT V559D/T670I (binding Kd: 13 nM)[21]. However, although compounds **2**-**6** could overcome the c-KIT T670I mutant, none of them could achieve the selectivity between the c-KIT wt and T670I mutant. Given the fact that c-KIT wt plays important roles in normal physiological functions, inhibitors that are selectively potent to the c-KIT mutant over c-KIT wt would provide potential better therapeutic window. This concept has been successfully demonstrated by the third generation EGFR inhibitor osimertinib, which selectively inhibits the EGFR T790M mutant over the EGFR wt.[22] Based on the binding conformation of kinases, kinase inhibitors can be categorized as type I binding mode which features a DFG-in kinase active conformation and type II binding mode which characterizes a DFG-out kinase inactive conformation.[23] Considering the potential chemical spaces for SAR exploration, the c-KIT wt/T670I dual inhibitor **6** was chosen as a starting point for further medicinal chemistry study. Through a fragment hybrid type II kinase inhibitor design approach[24], we have discovered a novel type II c-KIT kinase inhibitor compound **24** (CHMFL-KIT-033), which not only overcomes the c-KIT T670I mutant, but also achieved 12-fold selectivity over the c-KIT wt (Figure 2).

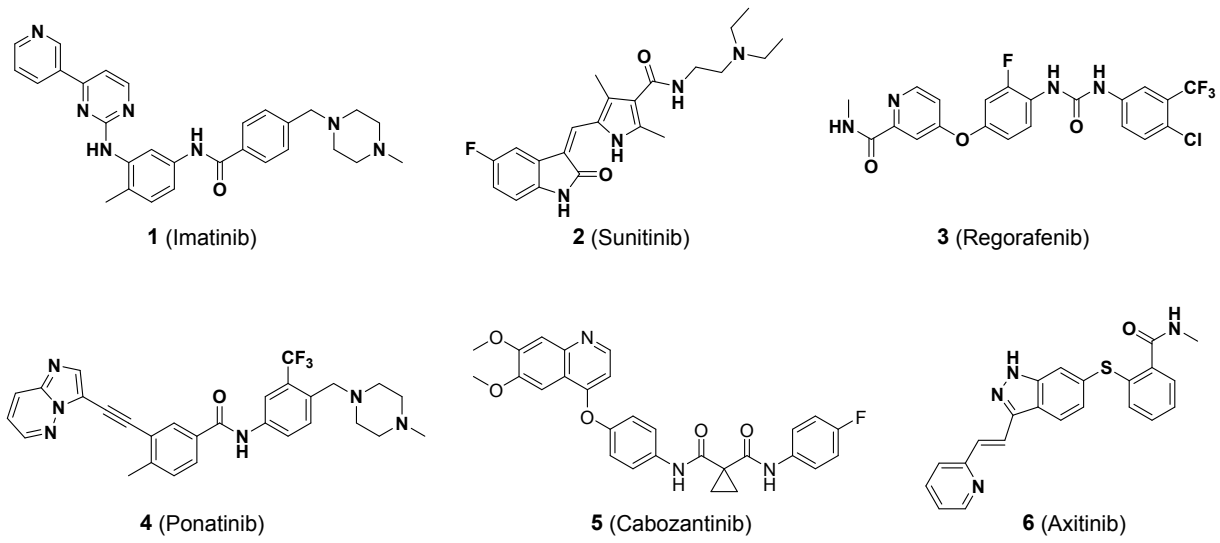

Figure 1. Chemical structures of representative c-KIT kinase inhibitors.

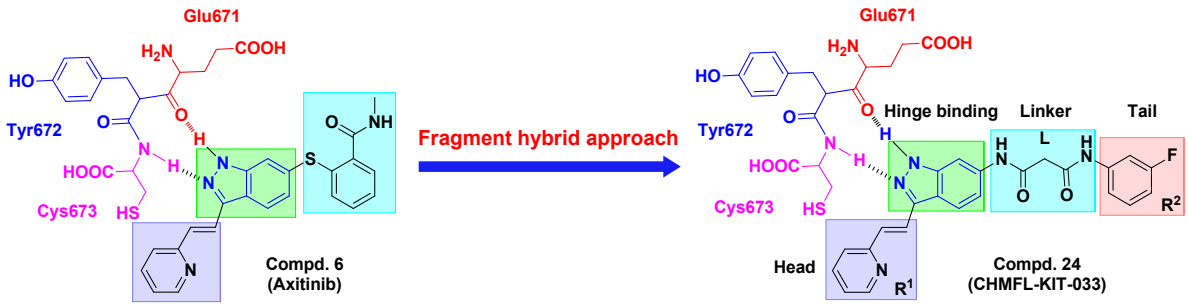

Figure 2. Schematic illustration of discovery of compound **24**.

RESULTS AND DISCUSSION

Design rationale and structure–activity relationship (SAR) exploration.

Currently there is no available X-ray crystal structure of compound **6** in complex with c-KIT kinase. Based on the published X-ray crystal structure of compound **6** in complex with the ABL kinase T315I mutant (PDB ID: 4TWP)[25], it might adopt type I binding mode with the c-KIT T670I mutant. However, based on the X-ray structure of compound **6** in complex with VEGFR2 kinase (PDB ID: 4AG8)[26], it might adopt type II binding mode. Therefore, in order to better understand the binding mechanism of compound **6** to c-KIT T670I, we first docked it to the DFG-in kinase active confirmation of c-KIT T670I (generated from PDB ID: 1PKG) using the Schrodinger induced fit docking protocol. The results showed that it could fit well in the DFG-in conformation and the indazole moiety formed two hydrogen bonds with Cys673 and Glu671 in the hinge binding area (Figure 3A). In addition, in the DFG-in conformation, the carbonyl group of benzamide formed a hydrogen bond with residue Asp810 in the DFG motif. Interestingly, we also found that compound **6** could fit well in the DFG-out kinase inactive conformation of c-KIT T670I (generated from PDB ID: 1T46, Figure 3B). In the DFG-out conformation, the NH of benzamide formed a hydrogen bond with Glu640 located in the αC-Helix. Considering that both c-KIT kinase and VEGFR2 kinase belong to type III receptor tyrosine kinase family and share

better structural similarity, we were prone to think that compound **6** adopted type II binding mode with c-KIT kinase. In addition, by comparing these two binding modes, we envisioned that there was limited space for affinity and selectivity improvement from type I binding mode. Given the bulky size of Ile670 residue, the inhibitor might need a more flexible linkage moiety. Meanwhile, the amino acid residues around the hydrophobic pocket that are generated by DFG-out shifting (shown in Figure 3C) are not conserved among different kinases and thus can serve as good factors to trim the selectivity for the type II inhibitors. Therefore, exploration of the type II binding mode, which further modifies the "linker" and "tail" moieties, might achieve the binding affinity and selectivity against the c-KIT T670I mutant. Based on this assumption, using the fragment hybrid type II kinase inhibitor design approach, we first designed compound **7** by replacing the thiol linkage in compound **6** with the malonamide which presumably would provide more space to accommodate the larger isoleucine residue, and then docked it to the DFG-out conformation of c-KIT T670I (generated from PDB ID: 1T46, Figure 3D). As expected, the docking results demonstrated that compound **7** prefers to adopt a typical type II binding mode which features two canonical hydrogen bonds formed between Glu640 and Asp810 with the amide in the linker. The indazole core forms two hydrogen bonds with Cys673 and Glu671 in the hinge binding area and the "tail" moiety 4-chloro-3-trifloromethylphenyl occupies the hydrophobic pocket (Figure 3E). The "head" moiety vinylpyridine occupies the shallow hydrophobic groove adjacent to the hinge binding area (Figure 3F). On the basis of these analyses and the fragment hybrid type II kinase inhibitor design approach[23,24], we started to explore the SAR by varying the "head", "linker" and "tail" moieties meanwhile keeping the indazole core scaffold of compound **7**.

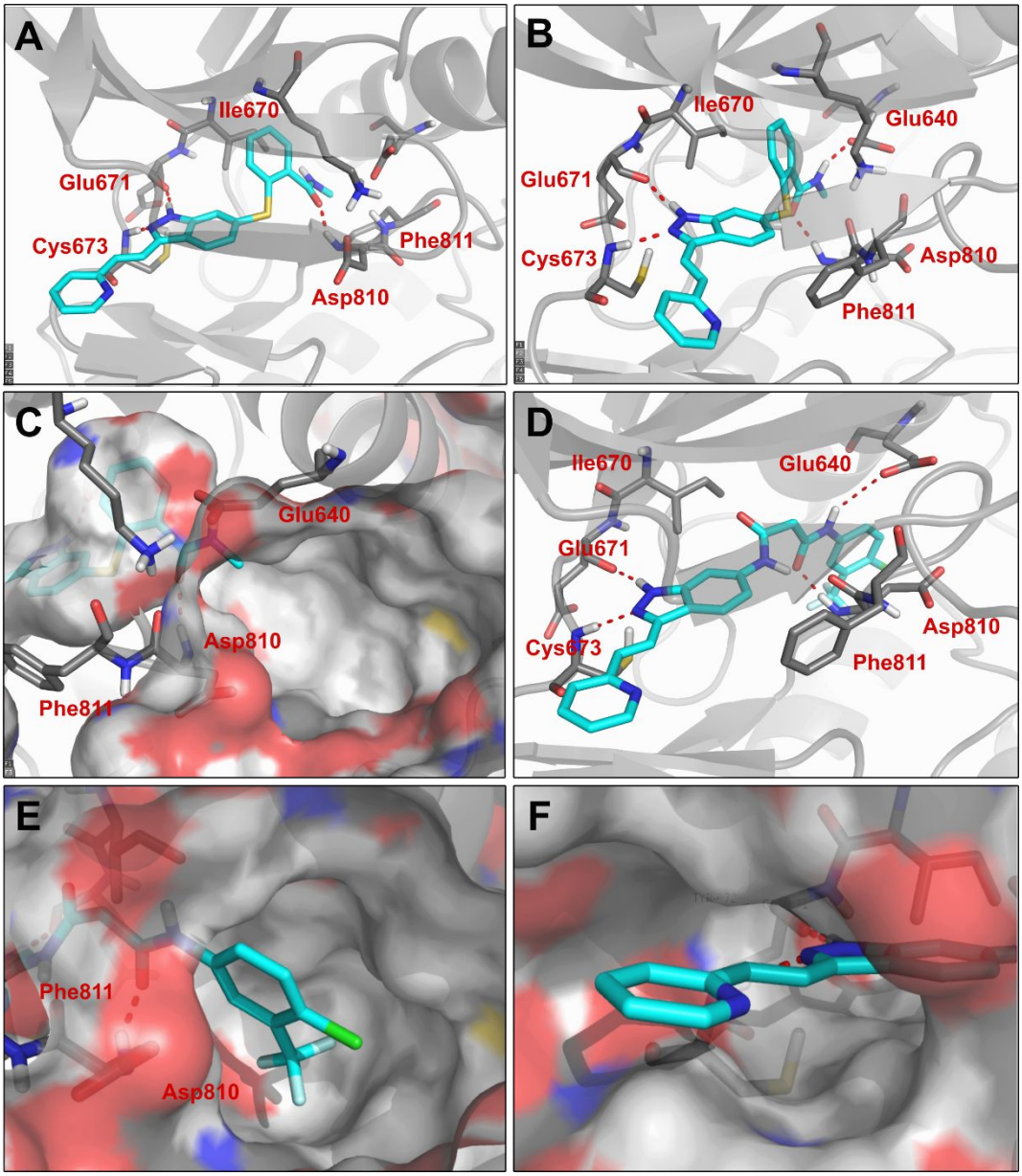

Figure 3. Schematic illustration of the SAR exploration rationale. (A) Type I binding mode of compound **6** with c-KIT T670I (generated from PDB code 1PKG). (B) Type II binding mode of compound **6** with c-KIT T670I (generated from PDB code 1T46). (C) Surface illustration of the hydrophobic pocket created by the DFG-out flip of c-KIT T670I (generated from PDB code 1T46). (D) Binding mode of compound **7** with c-KIT T670I (generated from PDB code 1T46).

(E) Surface illustration of the hydrophobic pocket created by the DFG-out flip of c-KIT T670I. (F) Surface illustration of the shallow hydrophobic groove adjacent to the hinge binding area.

We used the proliferation of IL-3 independent BaF3 cells expressing the c-KIT wt (BaF3-tel-c-KIT) and c-KIT T670I (BaF3-tel-c-KIT-T670I) as the primary readout to evaluate the compound's activity and selectivity. As the starting point, we first explored the SAR of the "linker" part (L). Replacement of the phenyl thiol ether linkage with malonamide linkage (**7**) resulted in improved potency against both c-KIT wt ($GI_{50:}$ 0.025 μM) and c-KIT T670I (GI_{50}: 0.002 μM) compared to compound **6**, meanwhile exhibited 12-fold selectivity between c-KIT T670I and c-KIT wt (Table 1). In addition, there is also a good selectivity window over the parental BaF3 cells (GI_{50}: 7.4 μM) indicating a good on-target antiproliferative inhibition effect in the c-KIT wt and c-KIT T670I transformed BaF3 cells. This result indicated that the design approach of type II kinase inhibitor from compound **6** was valid. However, shorter linkers such as amide (**8**), ethyleneamide (**9**) and urea (**10**) all resulted in activity loss against c-KIT T670I. Restoring the length of the linker but increasing the size by adding the cyclopropyl group to the linker (**11**) also led to activity loss to both c-KIT wt and c-KIT T670I.

Table 1. SAR Exploration Focused on the Linker Moiety (L)[a]

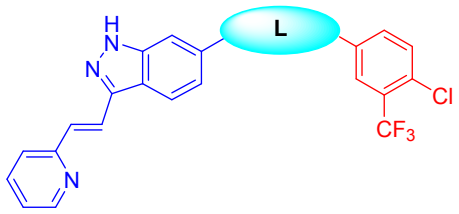

Compd.	Linker (L)	BaF3 (GI_{50}: μM)	BaF3-tel-c-KIT (GI_{50}: μM)	BaF3-tel-c-KIT-T670I (GI_{50}: μM)

6	-	1.64	0.105	0.108
7	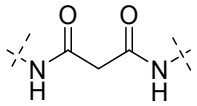	7.4	0.025	0.002
8	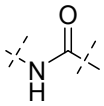	1.71	2.97	1.71
9	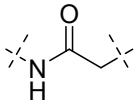	3.79	5.5	3.18
10	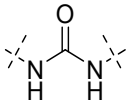	1.9	1.6	1.15
11	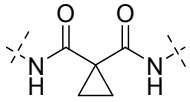	>10	1	0.23

[a]All GI_{50} values were obtained by triplet testing.

We then fixed the "linker" moiety as malonamide and explored the "head "moiety R^1 (Table 2). Replacement of the vinyl pyridine of **7** with hydrogen (**12**) and methyl group (**13**) both led to significant activity loss. However, 1-methyl-1*H*-pyrazole (**14**), pyridine (**15**) and 2-methylpyridine (**16**) all resulted in good inhibitory activities against c-KIT T670I (GI_{50}: 0.023 μM, 0.045 μM and 0.059 μM, respectively) meanwhile achieved the selectivity of c-KIT T670I over c-KIT wt ranging from 7- to 15-fold. This indicated that the aromatic moieties in the "head" region played an important role for the binding with c-KIT kinase. Changing the R^1 moiety from the pyridine in **15** to 5-(methylcarbamoyl)pyridin (**17**), fluorophenyl (**18**) and 3-carbamoylphenyl (**19**) all led to activity loss against c-KIT wt and c-KIT T670I. *N*-methyl formamyl (**20**) at R^1 also exhibited good activity against c-KIT T670I (GI_{50}: 0.057 μM) and 6-fold selectivity over c-

KIT wt. Larger groups such as 4-*N*-methyl piperazine (**21**) and *N*-methyl piperazinyl methylene (**22**) groups both resulted in much more potent activity against c-KIT T670I and c-KIT wt but also exhibited inhibitory activity to parental BaF3 cells. All these results indicated that the vinyl pyridine moiety at the R^1 position (as in compound **7**) was preferred because it exhibited the best potency against c-KIT T670I and better selectivity over c-KIT wt.

Table 2. SAR Exploration Focused on the Head Moiety (R^1)[a]

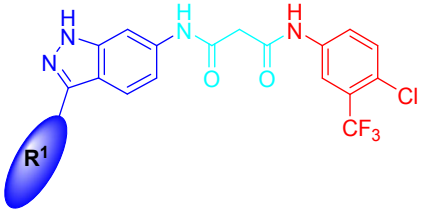

Compd.	Head (R^1)	BaF3 (GI_{50}: μM)	BaF3-tel-c-KIT (GI_{50}: μM)	BaF3-tel-c-KIT-T670I (GI_{50}: μM)
12	H	>10	>10	2.67
13	Me	>10	>10	1.88
14	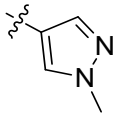	>10	0.35	0.023
15	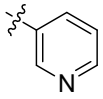	>10	0.32	0.045
16	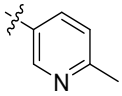	4.91	0.183	0.059

17	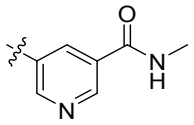	>10	>10	4.84
18	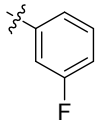	>10	1.12	0.179
19	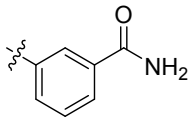	>10	1.55	0.339
20	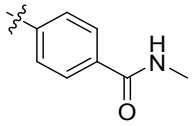	>10	0.338	0.057
21	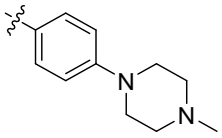	1.35	0.025	0.012
22	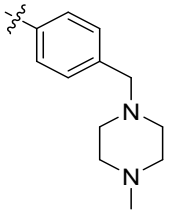	0.911	0.019	0.012

[a]All GI_{50} values were obtained by triplet testing.

We next explored the "tail" (R^2) moiety by fixing the "head" as vinyl pyridine and "linker" as malonamide (Table 3). Replacement of the R^2 moiety in compound **7** with a simple phenyl group (**23**) resulted in significant activity loss against c-KIT T670I (GI_{50}: 0.117 μM) but exhibited selectivity over c-KIT wt (19-fold). Encouraged by this result, we tried a series of *meta*-halogen substituted phenyl groups at R^2 to increase the hydrophobicity (**24**-**26**) and *m*-fluoro (**24**) exhibited the best potency against c-KIT T670I (GI_{50}: 0.044 μM) as well as the best selectivity over c-KIT wt (26-fold). Subsequently we tested a series of larger substituent groups such as *m*-methyl (**27**), *m*-methoxyl (**28**), *m*-*N*,*N*-dimethyl (**29**) and *m*-trifluoromethyl (**30**). However, all of

them exhibited decreased activity to c-KIT T670I and lower selectivity over c-KIT wt. The even larger group *m*-*N*-methyl piperazinyl (**31**) resulted in significant activity loss. Since *m*-fluorobenzene moiety at R^2 displayed the best activity, we also tried a series of fluoro-containing groups such as *o*-fluoro (**32**), *p*-fluoro (**33**) and some multi-fluoro substituents (**34-36**). However, all of them exhibited activity loss against c-KIT T670I compared to compound **24**.

Table 3. SAR Exploration Focused on the Tail Moiety (R^2)[a]

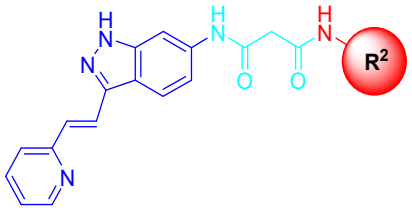

Compd.	Tail (R^2)	BaF3 (GI_{50}: μM)	BaF3-tel-c-KIT (GI_{50}: μM)	BaF3-tel-c-KIT-T670I (GI_{50}: μM)
23		6.72	2.22	0.117
24	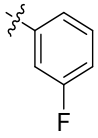	3.97	1.15	0.044
25	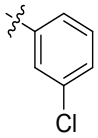	3.61	0.923	0.111
26	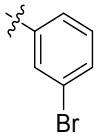	6.09	0.943	0.113
27	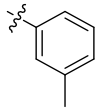	>10	1.43	0.17

28	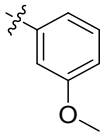	>10	2.74	0.234
29	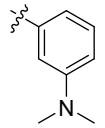	>10	3.87	0.594
30	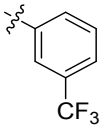	>10	0.216	0.086
31	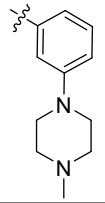	>10	>10	6.17
32	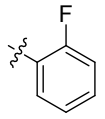	5.09	2.16	0.312
33	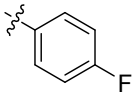	5.86	0.554	0.111
34	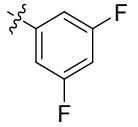	4.24	1.87	0.399
35	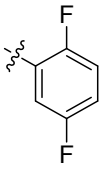	5.08	3.46	0.847
36	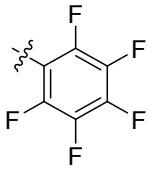	3.68	2.95	1.3

[a]All GI_{50} values were obtained by triplet testing.

Further biochemical and selectivity characterization of compound 24

Since compound **24** displayed the best combined potency and selectivity profiles against the c-KIT wt and T670I mutant, we then further examined its activity against a panel of c-KIT mutants in the c-KIT mutants transformed BaF3 cells (Table 4). Compared with compound **1**, **24** exhibited similar activities against primary gain-of-function mutations in the juxtamembrane domain such as V559D/A/G and L576P. Furthermore, **24** displayed 26-fold selectivity between c-KIT wt and c-KIT T670I in the BaF3 screening system compared with compound **6**. In addition, **24** exhibited better potencies against compound **1** resistant secondary mutants such as V654A and T670I in the ATP binding pocket. However, just as compound **1**, **24** did not show potent activities against activation loop mutations either. Comparably, compound **6** was potent against the c-KIT primary gain-of-function mutations and ATP binding pocket mutations but relatively resistant to the activation loops mutations. More importantly, there was no selectivity between the c-KIT wt and c-KIT T670I mutation.

Table 4. Antiproliferative effects of compounds **1**, **6** and **24** against a panel of c-KIT mutants transformed BaF3 cells.

GI_{50} (μM)	Mutated region	**1**	**6**	**24**
BaF3-tel-c-KIT	wt	0.364	0.105	1.15
BaF3-tel-c-KIT-V559D	Juxtamembrane	0.039	0.012	0.008
BaF3-tel-c-KIT-V559A	Juxtamembrane	0.005	0.005	0.031
BaF3-tel-c-KIT-V559G	Juxtamembrane	0.001	0.002	0.026
BaF3-tel-c-KIT-L576P	Juxtamembrane	0.115	0.007	0.157
BaF3-tel-c-KIT-V654A/V559D	ATP binding pocket	1.57	0.013	0.265

BaF3-tel-c-KIT-V654A	ATP binding pocket	2.30	0.014	0.525
BaF3-tel-c-KIT-T670I	ATP binding pocket	>10	0.108	0.044
BaF3-tel-c-KIT-T670I/V559D	ATP binding pocket	>10	0.129	0.122
BaF3-tel-c-KIT-D816V	Activation loop	>10	2.02	3.46
BaF3-tel-c-KIT-D816H	Activation loop	0.823	1.82	6.84
BaF3-tel-c-KIT-D820E	Activation loop	0.267	0.156	0.868
BaF3-tel-c-KIT-N822K	Activation loop	1.29	1.72	6.06
BaF3-tel-c-KIT-A829P	Activation loop	0.406	0.406	6.00

[a]All GI_{50} values were obtained by triplet testing.

We then used the Z'-LYTE based biochemical activity assay with purified kinase proteins to confirm the inhibition activities of compound **24** against the c-KIT wt and c-KIT T670I kinases. The results showed that **24** inhibited the c-KIT T670I kinase with an IC_{50} of 45 nM and inhibited the c-KIT wt kinase with an IC_{50} of 536 nM (Figure 4A). Compound **24** exhibited about 12-fold selectivity against c-KIT T670I over c-KIT wt. In order to further confirm this selectivity in cells, we proceeded to examine the phosphorylation of c-KIT at Y703, 719 and 823 sites in the colon cancer cell line COLO320DM which expresses c-KIT wt kinase. As expected, **24** did not apparently affect all of these three phosphorylation sites up to 1 μM (EC_{50}s: >1 μM) (Figure 4B). Similarly, in the c-KIT wt transformed BaF3 cells, **24** did not affect these c-KIT phosphorylation sites up to 1 μM (EC_{50}s >1 μM) either (Figure 4C). However, in the c-KIT T670I transformed BaF3 cells, **24** could potently inhibit the phosphorylation of c-KIT at Y703, 719 and 823 sites (EC_{50s}: 77 nM, 750 nM and 34 nM, respectively) (Figure 4D). The results demonstrated that both

in protein level and in cellular level, **24** could achieve the selectivity between c-KIT wt and c-KIT T670I, which further confirmed the selective antiproliferative effects observed from the transformed BaF3 cells.

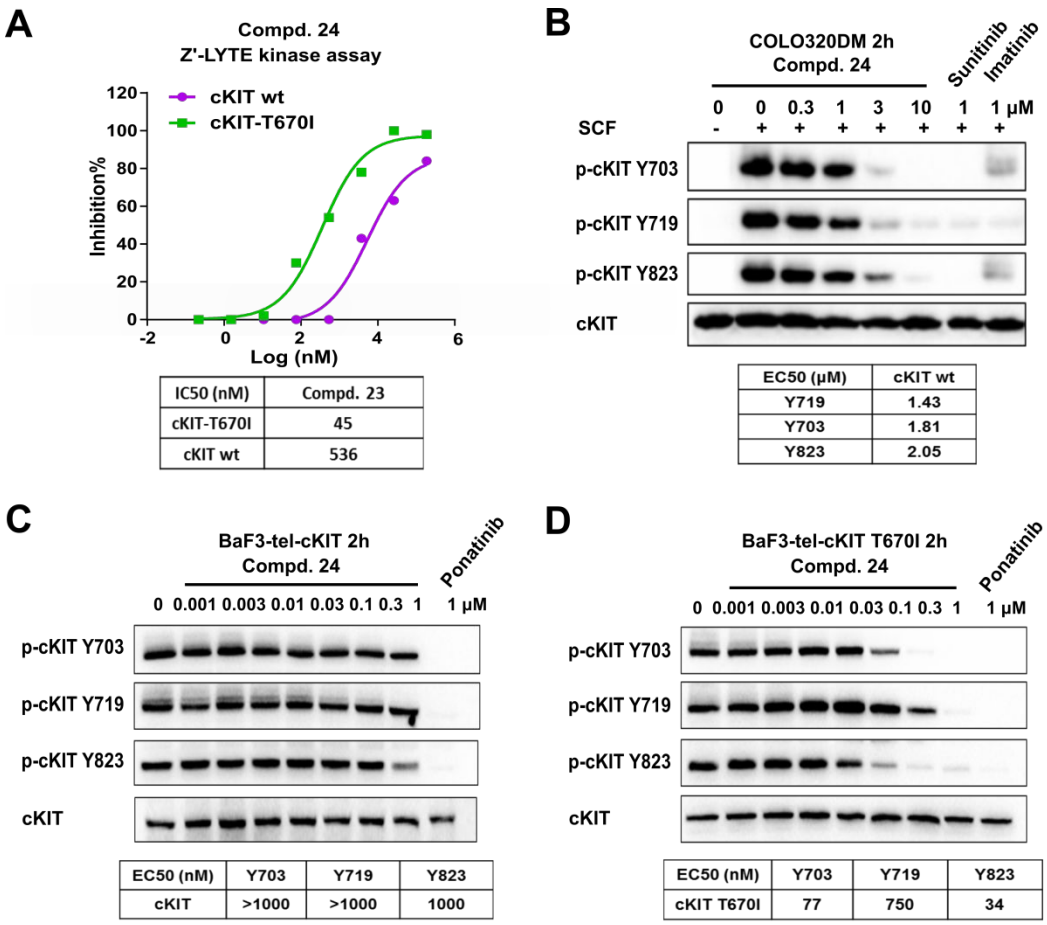

IC50 (nM)	Compd. 23
cKIT-T670I	45
cKIT wt	536

EC50 (μM)	cKIT wt
Y719	1.43
Y703	1.81
Y823	2.05

EC50 (nM)	Y703	Y719	Y823
cKIT	>1000	>1000	1000

EC50 (nM)	Y703	Y719	Y823
cKIT T670I	77	750	34

Figure 4. (A) Z'-LYTE biochemical kinase assay characterization of compound **24** against c-KIT wt/T670I kinases. (B) Inhibitory activity of **24** to the phosphorylation of c-KIT wt in the colon cancer cell line COLO320DM. (C) Inhibitory activity of **24** to the phosphorylation of c-KIT wt in BaF3-tel-c-KIT cells. (D) Inhibitory activity of **24** to the phosphorylation of c-KIT T670I in BaF3-tel-c-KIT-T670I cells.

To further characterize the selectivity of compound **24** among other protein kinases, we examined its kinome-wide selectivity profile with DiscoverX's KINOMEscan binding

technology[21] (Figure 5). The results demonstrated that **24** bore a good selectivity (S score (1) = 0.02) in a panel of 468 kinases and mutants at 1 μM concentration (Figure 5A). Besides high binding affinity to c-KIT kinase, it also displayed strong binding to CSF1R, CSNK1A1, NEK, PAK2, PDGFRβ, PIM and YSK1 kinases (percent of control value less than 1% at 1 μM. For further details, please refer to https://www.discoverx.com/services/drug-discovery-development-services/kinase-profiling/kinomescan/scanelect) (Figure 5 and Supplementary Table 1). In addition, among the c-KIT mutant panel in the assay, **24** exhibited strong binding to c-KIT L576P, V559D, V559D/T670I and V559D/V654A (%Ctrl value less than 1% at 1 μM) which was consistent with the results observed from the transformed BaF3 cells in Table 4. Given the fact that KINOMEscan is a binding assay, which sometimes may not reflect the real inhibitory activity of the compound, we also used the Z'-LYTE activity-based assay to test the inhibitory activity of **24** against these potential targets revealed by KINOMEscan assay. The data showed that **24** could also potently inhibit CSF1R kinase (IC_{50} = 14.2 nM) besides c-KIT T670I (Figure 5C). This could be explained that both of c-KIT T670I and CSF1R belong to the type III receptor tyrosine kinase family and the ATP pocket of these two kinases are highly conserved. Interestingly, **24** did not show potent inhibitory activity against other targets from KINOMEscan assay such as CSNK1A1, NEK1, PAK2, PDGFR, PIM3 and STK25, indicating that **24** was only selectively potent toward c-KIT T670I mutant and CSF1R kinase.

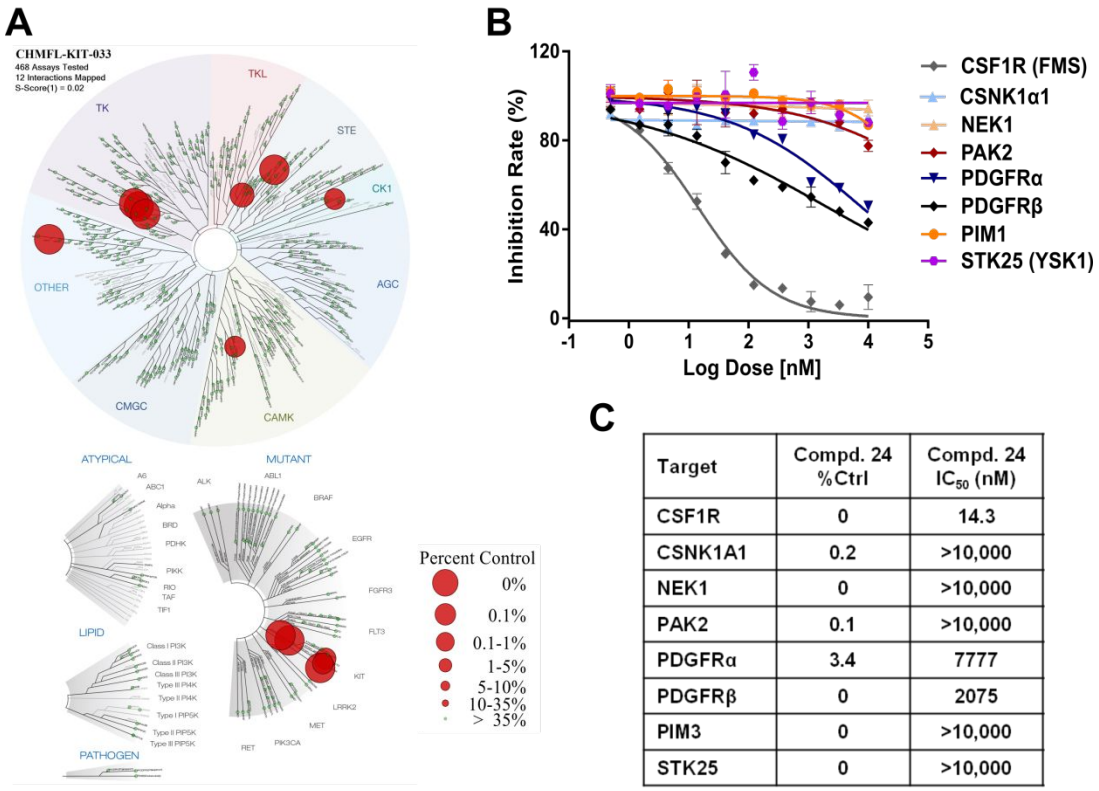

C

Target	Compd. 24 %Ctrl	Compd. 24 IC_{50} (nM)
CSF1R	0	14.3
CSNK1A1	0.2	>10,000
NEK1	0	>10,000
PAK2	0.1	>10,000
PDGFRα	3.4	7777
PDGFRβ	0	2075
PIM3	0	>10,000
STK25	0	>10,000

Figure 5. Kinome-wide selectivity profiling of compound **24**. (A) KINOMEscan profiling of **24** at a concentration of 1 μM against 468 kinases and mutants. (B) and (C) Z'-LYTE kinase assay of **24** against the kinase targets revealed from the KINOMEscan profiling in isogenic cell lines. The table shows the target kinases that remained activity of less than 1% control in the presence of 1 μM of **24** and the IC_{50} values of these kinases.

In order to better understand its binding mechanism, we then docked it into the c-KIT wt (PDB code: 1T46) and T670I mutant kinase (generated from PDB code: 1T46) by molecular modeling. In the c-KIT wt (PDB code: 1T46) model, **24** adopts a canonical type II binding mode. The two nitrogen atoms of indazol form two hydrogen bonds with the c-KIT residues Cys673 and Glu671 in the hinge binding area (Figure 6A). The amide in the linker moiety forms two hydrogen bonds with Glu640 located in the c-helix and Asp810 in the DFG motif. The "tail" part occupies the hydrophobic pocket generated by the DFG-out shifting. In the homology model of c-KIT T670I

mutant, **24** adopts a similar type II binding mode. The malonamide linkage is flexible which generates enough space to accommodate the larger residue Ile670, which could explain its potency against the T670I mutant (Figure 6B). However, the modeling study from the published and homology structures could not explain the selectivity between the c-KIT wt and c-KIT T670I, we reasoned that there might be some kinetic factors that associate with T670I mutant[27,28] or the drug binding might induced special conformational change either in the c-KIT wt or c-KIT T670I mutant which makes the inhibitor **24** more favorable for c-KIT T670I. All of these speculations would require further detailed kinetic and structural biology studies.

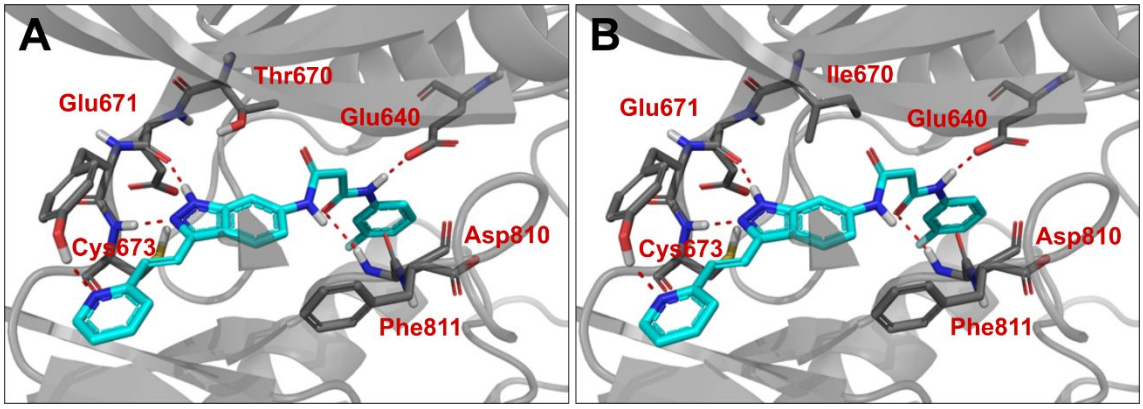

Figure 6. Schematic illustration of the binding mechanism of compound **24**. (A) Binding mode of **24** with c-KIT wt (PDB code: 1T46). (B) Binding mode of **24** with c-KIT T670I (generated from PDB code: 1T46).

In Cell Evaluation of Compound 24.

We next investigated the antiproliferative effects of compound **24** against a panel of established GISTs cancer cell lines (Table 5). Compound **24** was potent against GIST-T1 (c-KIT del 560-578, GI_{50}: 0.052 μM) and moderately potent against GIST882 (c-KIT K642E, GI_{50}: 0.296 μM) cell lines. In the compound **1**-resistant cell line GIST-T1-T670I (c-KIT T670I, generated by CRISPR-Cas9 knock-in T670I mutant to the GIST-T1 cell line) (GI_{50}>10 μM), **24**

displayed a GI_{50} value of 0.288 μM. In addition, in another compound **1**-resistant cell line GIST-5R (c-KIT T670I, generated by continuous treatment of **1** and colon selection), **24** also exhibited better antiproliferative effects than **1** (GI_{50}: 0.475 μM versus 10 μM). Neither of these two inhibitors has effect against GIST-48B cell line which is c-KIT independent.

Table 5. Antiproliferative effects of compounds **1** and **24** against GIST cells.

Cell line	c-KIT status	Compd. **1** (GI_{50}: μM)	Compd. **24** (GI_{50}: μM)
GIST-T1	Δ560-578	0.026	0.052
GIST-882	K642E	0.058	0.296
GIST-T1-T670I	Δ560-578/T670I	>10	0.288
GIST-5R	Δ560-578/T670I	>10	0.475
GIST-48B	c-KIT-independent	>10	>10

[a]All GI_{50} values were obtained by triplet testing.

We also evaluated the effect of compound **24** to the c-KIT-mediated signaling pathways in the GISTs cancer cell lines (Figure 7). As expected, **24** potently inhibit the c-KIT autophosphorylation sites p-Y719, p-Y703, p-Y823 and downstream signaling mediators such as p-AKT (S473), p-ERK (T202/Y204) and p-S6 (S235/S236) starting from 0.1 μM concentration in the c-KIT growth-dependent GISTs cancer cell line GIST-T1 and two compound **1**-resistant cell lines GIST-T1-T670I and GIST-5R (Figure 7A). Interestingly, in the GIST-T1-T670I and GIST-5R cells, compound **24** but not **1** could inhibit the phosphorylation of STAT3 dose-dependently. While in the GIST-T1 cells, neither **24** nor **1** could affect the phosphorylation of

STAT3. In accordance with the effect of **24** on the c-KIT-mediated signaling pathways, **24** could also induce the cell cycle arrest and apoptosis dose-dependently in these cell lines (Figure 7B, C).

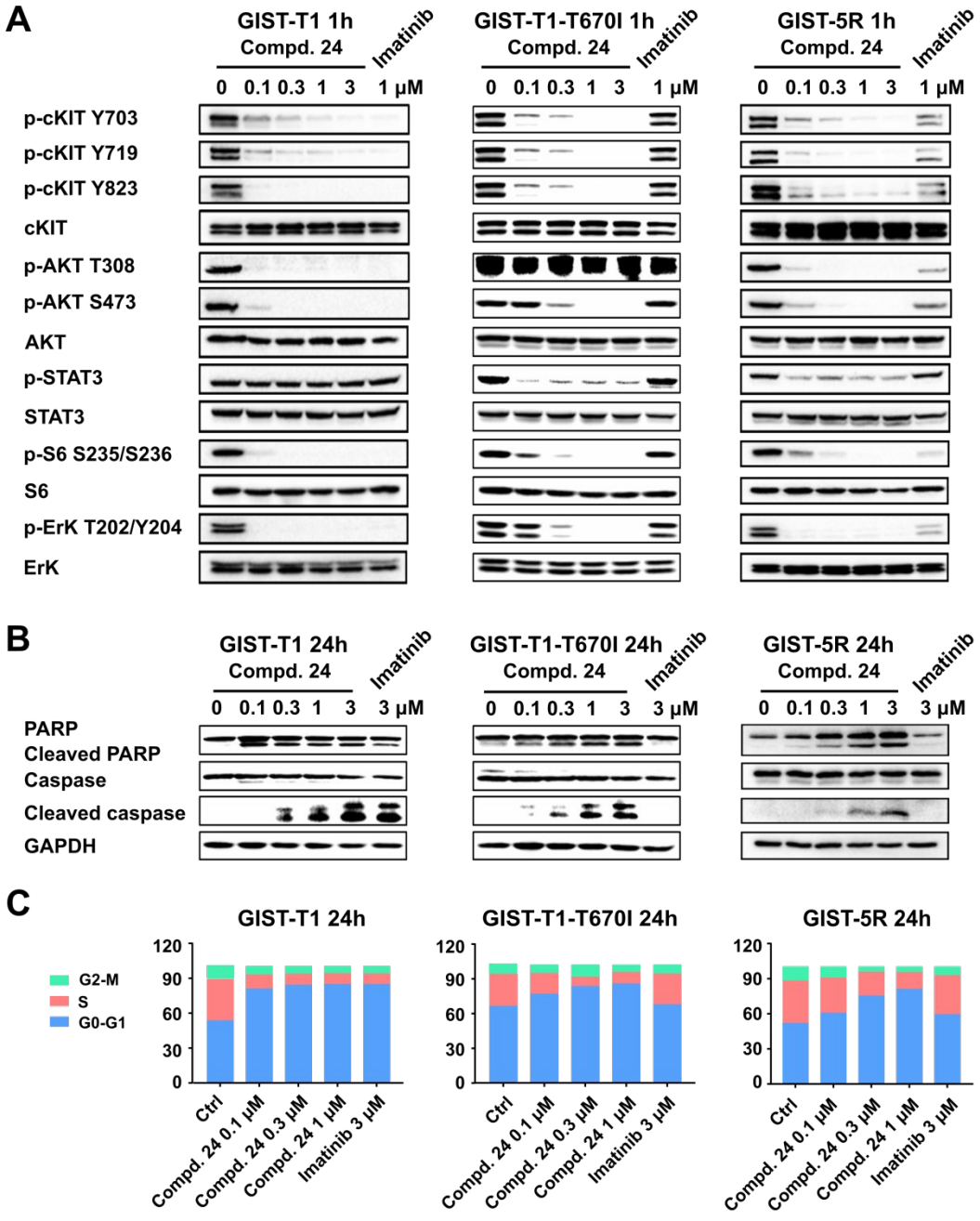

Figure 7. Characterization of the cellular effects of compound **24.** (A) Effects of **24** on the c-KIT-mediated signaling transduction pathways in GIST-T1, GIST-T1-T670I and GIST-5R cells after 1 h inhibitor treatment. (B) Apoptosis induction effects of **24** in GIST-T1, GIST-T1-T670I

and GIST-5R cells after 24 h inhibitor treatment. (C) Cell cycle arresting effects of **24** in GIST-T1, GIST-T1-T670I and GIST-5R cells after 24 h inhibitor treatment.

In vivo PK/PD Evaluation

We then examined the in vivo PK profile of compound **24** in rats and mice following intravenous and oral administration (Table 6). The results demonstrated that in rats **24** displayed an acceptable bioavailability (F = 27.5%) with a relatively longer half-life ($T_{1/2}$ = 4.9 h) and moderate drug exposure (AUC_{0-t} = 712 ng/mL·h) with 10 mg/kg of oral administration. While in mice **24** exhibited a bioavailability of 16.4% with good drug exposure (AUC_{0-t} = 1469 ng/mL·h) and moderate half-life ($T_{1/2}$=1.6 h). These data indicated that the oral administration of **24** was acceptable for the in vivo efficacy study.

Table 6. Pharmacokinetic Study of Compound **24** on Rats and Mice[a]

Compd. **24**	Rats		Mice	
	I.V. (1 mg/mg)	P.O. (10 mg/mg)	I.V. (1 mg/mg)	P.O. (10 mg/mg)
$AUC_{(0-t)}$ (ng/mL·h)	258.9±30.6	712.5±172.5	897.9	1468.9
$AUC_{(0-\infty)}$ (ng/mL·h)	307.2±27.1	808.9±46.8	901.4	1478.3
T_{max} (h)	0.017±0	1.7±2.1	0.03	0.5
$T_{1/2}$ (h)	10.4±1.5	4.9±0.5	4.9	1.6
Vz (L/kg)	49.3±10.3	86.8±11.8	5.7	19.0
CLz (L/h/kg)	3.3±0.3	12.4±0.7	1.1	6.8
C_{max} (ng/mL)	378.5±104.4	97.1±27.9	3017.0	1124.0
$MRT_{(0-\infty)}$ (h)	6.4±0.3	5.4±1.9	0.4	2.2

F%	--	27.5	--	16.4

[a]All data were obtained by triple testing (±SD) except mice.

We also evaluated the pharmacodynamic profile of **24** in the GIST-5R mouse model at the 100 mg/kg/day dosage for the impact on levels of p-c-KIT and downstream markers p-ERK and p-AKT (Figure 8 and Supplementary Figure 1). Meanwhile, we also monitored the drug concentration in the blood plasma. Following a single dose treatment, in 2 h time course the levels of p-c-KIT/ERK/AKT decreased to lowest and then started to recover. The drug concentration in the plasma reached highest level in 30 min and then gradually decreased to basal levels in 4 h, which was correlated to the levels of phosphorylation of the signaling mediators.

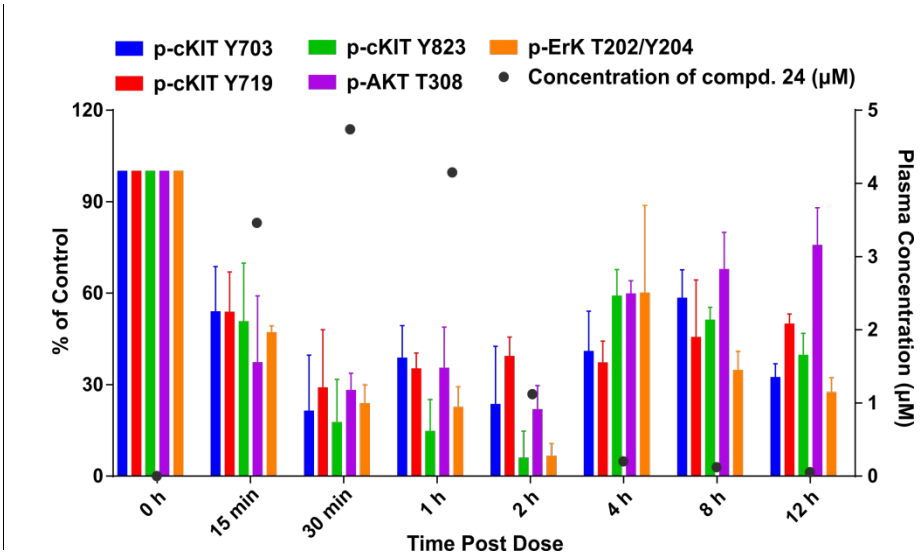

Figure 8. Pharmacodynamic effects of compound **24** on p-c-KIT, p-ErK and p-AKT in tumor from the GIST-5R xenograft mouse model with a single dosage of 100 mg/kg/day *p.o.* administration.

Finally, the in vivo antitumor efficacy of compound **24** was evaluated in the GIST-5R cells inoculated xenograft mouse model. Upon 28 days continuous oral gavage treatment, none of the 25, 50 and 100 mg/kg/day (QD) administration affected the mouse body weight (Figure 9A) and **24** dose-dependently inhibited the tumor growth (Figure 9B). The 100 mg/kg/day dosage achieved a tumor growth inhibition (TGI) of 83% (Figure 9C, D) which was much better than compound **1**.

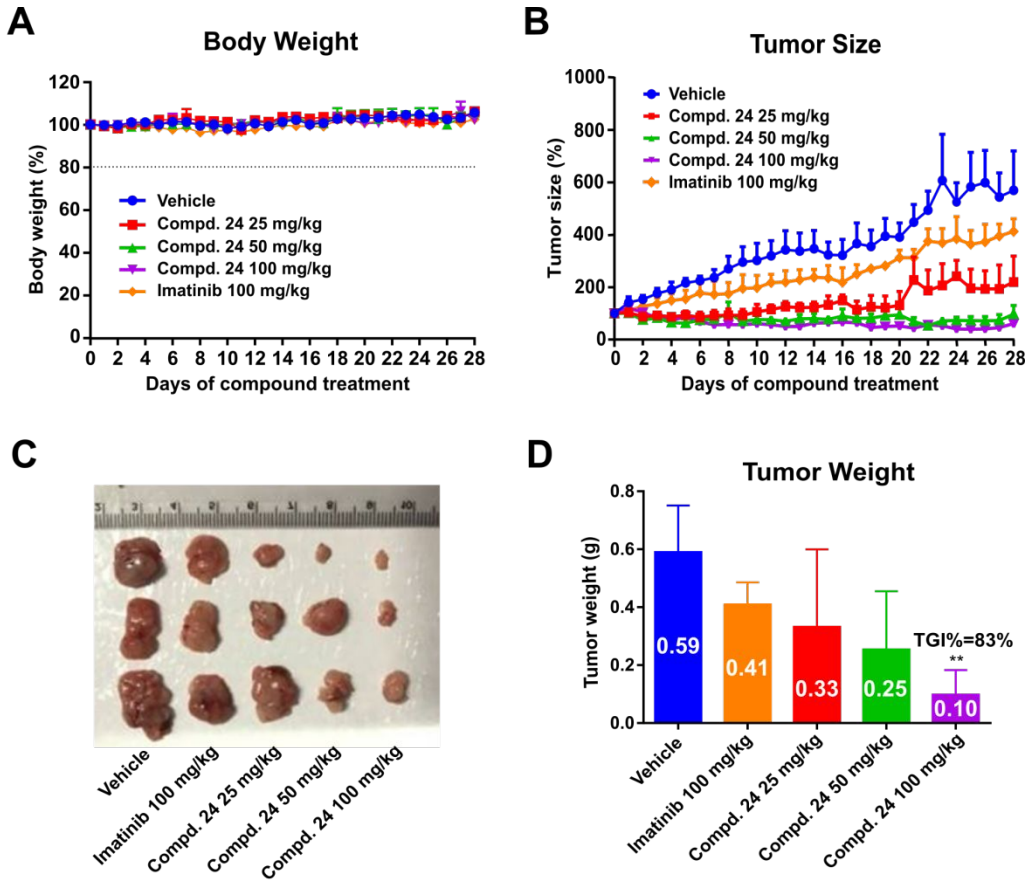

Figure 9. In vivo antitumor efficacy of compound **24** in the GIST-5R xenograft mouse model. Female nu/nu mice bearing established GIST-5R tumor were treated with **24** at 25, 50 and 100 mg/kg/d or vehicle control. Daily oral administration was initiated when GIST-5R tumors had reached a size of 200 mm^3. Each group contained 4 animals. Data = mean±SEM. (A) Body

weight change in mice for each daily dosing group of **24** and imatinib. Initial body weight was set as 100%. (B) Tumor size measurements of GIST-5R xenograft mice after **24** and imatinib treatment. (C) Representative photographs of tumors in each group after 25, 50, 100 mg/kg/d of **24** or vehicle treatment. (D) Comparison of the final tumor weight in each group of 28-day treatment period.

CHEMISTRY

The syntheses of **7**, **11** and **23-36** are illustrated in Scheme 1. Methyl ester **38** was obtained by amide coupling reaction of **37** with carboxylic acid. Then hydrolysis under basic condition afforded carboxylic acid **39.** Finally, amide coupling reaction with amine and removal of the tetrahydropyranyl (THP) protective group furnished the target compounds. As shown in Scheme 2, **8** and **9** were obtained from amide coupling reaction of **37** with carboxylic acid followed by deprotection of the THP group. To obtain **10**, **37** was first converted to urea and then the THP protective group was removed. In Scheme 3, Suzuki coupling reaction of **40** with arylboronic acid and protection of **41** with THP group afforded intermediate **42**. Then the nitro group was reduced to provide amine **43**. Coupling reaction of **44** with methyl hydrogen malonate followed by hydrolysis of methyl ester **45** offered carboxylic acid **46**. The final compounds **12-22** were obtained by amide coupling reaction of **43** with **46** and removal of the THP protective group.

Scheme 1. Synthetic Route of Compounds **7**, **11** and **23-36**[a]

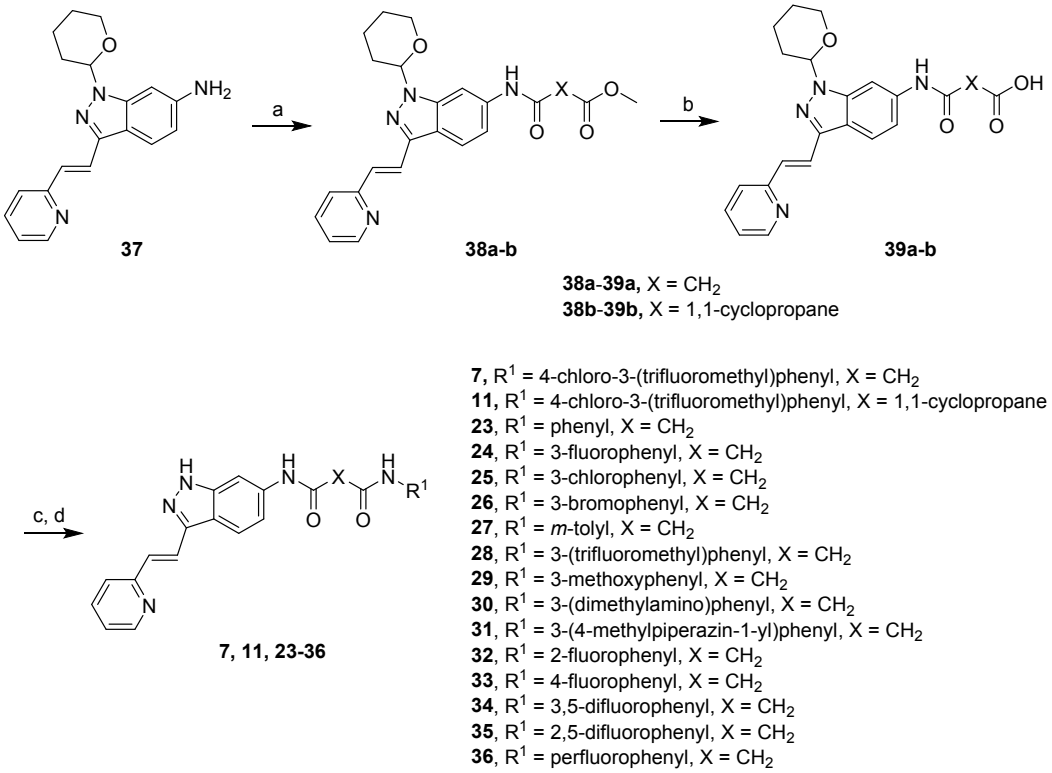

[a]Reagents and conditions: (a) methyl hydrogen malonate or 1,1-yclopropanedicarboxylic acid monomethyl ester, HATU, DIPEA, DMF, rt, 2 h; (b) LiOH, MeOH, H_2O, rt, 6 h; (c) R^1NH_2, HATU, DIPEA, DMF, rt, 2 h; (d) CF_3COOH, DCM, rt, 4 h.

Scheme 2. Synthetic Route of Compounds **8-10**[a]

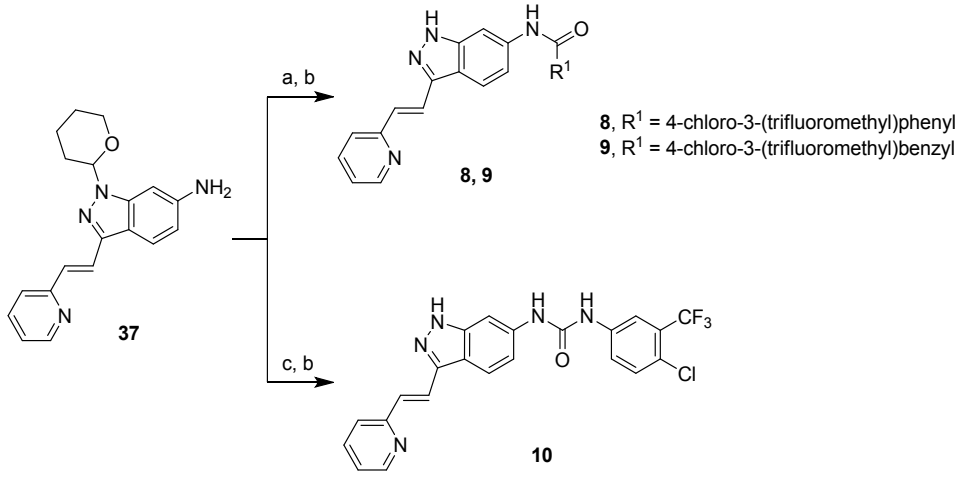

[a]Reagents and conditions: (a) 4-chloro-3-(trifluoromethyl)benzoic acid or 4-chloro-3-(trifluoromethyl)phenylacetic acid, HATU, DIPEA, DMF, rt, 2 h; (b) CF_3COOH, DCM, rt, 4 h; (c) 4-chloro-3-(trifluoromethyl)phenyl isocyanate, DCM, rt, 8 h.

Scheme 3. Synthetic Route of Compounds **12-22**[a]

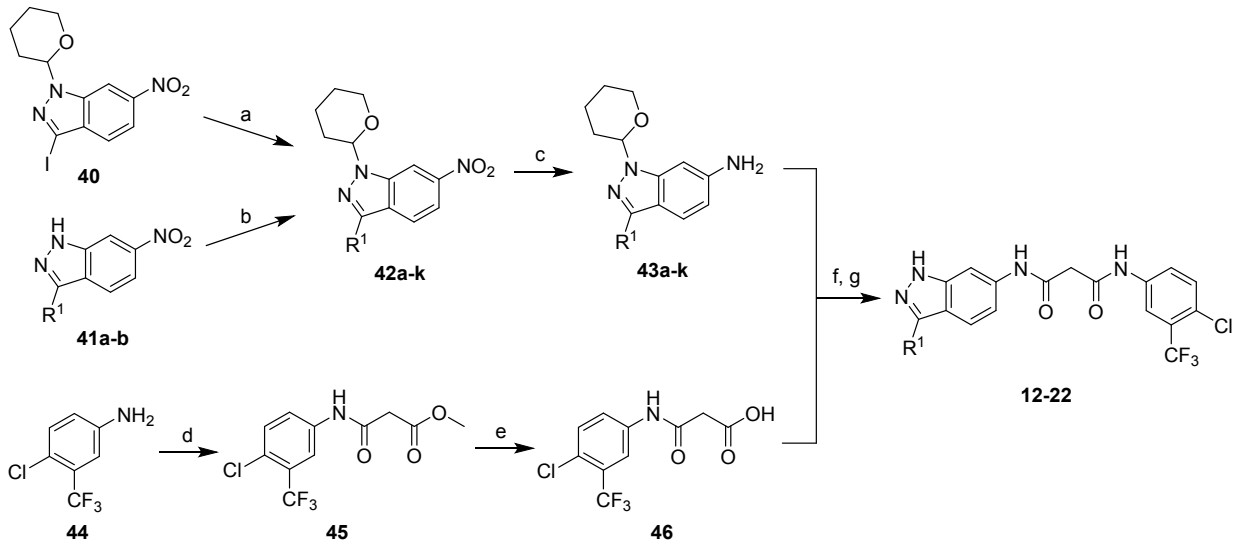

41a-43a, 12, R^1 = H
41b-43b, 13, R^1 = Me
42c-43c, 14, R^1 = methyl-1*H*-pyrazol-4-yl
42d-43d, 15, R^1 = pyridin-3-yl
42e-43e, 16, R^1 = 6-methylpyridin-3-yl
42f-43f, 17, R^1 = 5-(methylcarbamoyl)pyridin-3-yl
42g-43g, 18, R^1 = 3-fluorophenyl
42h-43h, 19, R^1 = 3-(3-carbamoylphenyl)
42i-43i, 20, R^1 = 3-(4-(methylcarbamoyl)phenyl
42j-43j, 21, R^1 = 3-(4-(4-methylpiperazin-1-yl)phenyl
42k-43k, 22, R^1 = 3-(4-((4-methylpiperazin-1-yl)methyl)phenyl

[a]Reagents and conditions: (a) arylboronic acid, $Pd(Ph_3P)_4$, K_2CO_3, 1,4-dioxane, H_2O, reflux, 12 h; (b) dihydropyran, CH_3SO_3H, THF, reflux, 8 h; (c) H_2, 10% Pd/C, MeOH, rt, 20 h; (d) methyl hydrogen malonate, HATU, DIPEA, DMF, rt, 2 h; (e) LiOH, MeOH, H_2O, rt, 6 h. (f) HATU, DIPEA, DMF, rt, 2 h; (g) CF_3COOH, DCM, rt, 4 h.

CONCLUSIONS

In summary, starting from a type I multiple kinase inhibitor **6** which displayed moderate c-KIT wt and c-KIT T670I dual inhibitory effects, through fragment hybrid drug design approach, we

discovered a novel indazole scaffold based c-KIT T670I mutant selective type II kinase inhibitor **24**. In the purified protein biochemical assay, transformed BaF3 cell growth inhibition assay and in cell on-target phosphorylation assay, **24** achieved 10-30-fold selectivity between c-KIT T670I and c-KIT wt. In addition, it also displayed great selectivity profile over other protein kinases in the kinome except CSF1R kinase. **24** exhibited potent antiproliferative effect against imatinib-sensitive GIST cell line GIST-T1 and imatinib-resistant cell lines GIST-T1-T670I and GIST-5R through potent inhibition of the c-KIT-mediated signaling pathways, arrest of the cell cycle progression and induction of the apoptosis. Furthermore, **24** displayed a suitable PK profile and potent in vivo antitumor efficacy. Although the selectivity mechanism of the inhibitor between the c-KIT T670I mutant and c-KIT wt remains to be elucidated, the high selectivity, in cell and in vivo properties of **24** might make it a useful pharmacological tool for the c-KIT wt/mutants associated physiological and pathological studies.

EXPERIMENTAL SECTION

Chemistry. All reagents and solvents were purchased from commercial sources and were used as received unless specified otherwise, or prepared as described in the literature. All moisture sensitive reactions were carried out using dry solvents under ultrapure argon protection. Glassware was dried in an oven at 140 °C for at least 12 h prior to use and then assembled quickly while hot, sealed with rubber septa, and allowed to cool under a stream of argon. Reactions were stirred magnetically using Teflon-coated magnetic stirring bars. Commercially available disposable syringes were used for transferring the reagents and solvents. LC/MS were performed on an Agilent 6224 TOF using an ESI source coupled to an Agilent 1260 Infinity HPLC system operating in reverse mode with an Agilent XDB-C18 column (4.6 × 50 mm, 1.8 μm) using a water/acetonitrile (each with 0.2% (v/v) formic acid) gradient at a flow rate at 0.5

mL/min. ^{1}H and ^{13}C spectra were recorded with a Bruker 400 MHz or 850 MHz NMR spectrometer. Chemical shifts are expressed in ppm. In the NMR tabulation, s indicates singlet; d, doublet; t, triplet; q, quartet and m, multiplet. Flash column chromatography was conducted using silica gel (Silicycle40−64 μm). The purities of all final compounds were determined to be above 95% by HPLC.

(E)-N^1-(4-Chloro-3-(trifluoromethyl)phenyl)-N^3-(3-(2-(pyridin-2-yl)vinyl)-1H-indazol-6-yl)malonamide (7). To a solution of **38a** (30 mg, 0.07 mmol) in DMF (5 mL) were added 4-chloro-3-(trifluoromethyl)aniline (15.6 mg, 0.08 mmol), HATU (41.8 mg, 0.11 mmol) and DIEPA (18.1 mg, 0.14 mmol). The resulting mixture was stirred at room temperature for 2 h. Then it was diluted with EtOAc (50 mL) and washed with water (100 mL × 3) and brine (100 mL). The organic layers were dried over anhydrous sodium sulfate and concentrated. The residue was diluted with DCM (1 mL) and CF_3COOH (0.5 mL). The reaction mixture was stirred at room temperature for 4 h and then the pH value was adjusted to 12 with saturated sodium bicarbonate. The mixture was extracted by EtOAc (50 mL) and washed with water (50 mL × 2) followed by brine (50 mL). The organic layers were dried over sodium sulfate and then filtered, concentrated and purified by silica gel column chromatography (eluting with 0−5% MeOH in DCM) to afford **7** as a yellow solid (17.5 mg, 53%). Yield = 48%. ^{1}H NMR (400 MHz, DMSO-d_6) δ 13.27 (s, 1H), 10.70 (s, 1H), 10.46 (s, 1H), 8.68 (s, 1H), 8.22 (d, J = 12.6 Hz, 2H), 8.14 (d, J = 8.6 Hz, 1H), 8.01 (d, J = 16.1 Hz, 2H), 7.87 (d, J = 7.7 Hz, 2H), 7.71 (d, J = 8.3 Hz, 1H), 7.59 (d, J = 16.4 Hz, 1H), 7.42 (s, 1H), 7.26 (d, J = 7.9 Hz, 1H), 3.59 (s, 2H); ^{13}C NMR (126 MHz, DMSO-d_6) δ 166.63, 165.81, 155.46, 149.96, 142.35, 142.22, 138.86, 137.86, 137.36, 132.72, 129.23, 127.12, 124.69, 124.54, 124.34, 123.00, 122.85, 121.51, 118.17, 117.63, 115.11, 99.74, 46.64; LC/MS (ESI, m/z) 500.11 $[M + H]^+$.

Compounds **8-9** and **11-36** were prepared following the synthetic procedure of compound **7**.

(E)-4-Chloro-N-(3-(2-(pyridin-2-yl)vinyl)-1H-indazol-6-yl)-3-(trifluoromethyl)benzamide (8) Yield = 52%. ^{1}H NMR (500 MHz, DMSO-d_6) δ 13.23 (s, 1H), 10.71 (s, 1H), 8.63 – 8.58 (m, 1H), 8.44 (s, 1H), 8.33 – 8.26 (m, 2H), 8.19 (d, J = 8.7 Hz, 1H), 7.99 – 7.91 (m, 2H), 7.82 (td, J = 7.6, 1.8 Hz, 1H), 7.68 (d, J = 8.7 Hz, 1H), 7.59 – 7.55 (m, 1H), 7.50 (d, J = 8.8 Hz, 1H), 7.28 (dd, J = 7.5, 1.0 Hz, 1H); ^{13}C NMR (126 MHz, DMSO-d_6) δ 163.94, 155.49, 150.00, 142.28, 142.23, 137.68, 137.32, 134.63, 134.42, 133.92, 132.42, 129.35, 127.62, 127.03, 124.65, 122.99, 122.86, 122.05, 121.35, 118.03, 116.23, 101.26; LC/MS (ESI, m/z) 443.09 $[M + H]^+$.

(E)-2-(4-Chloro-3-(trifluoromethyl)phenyl)-N-(3-(2-(pyridin-2-yl)vinyl)-1H-indazol-6-yl)acetamide (9) Yield = 55%. ^{1}H NMR (500 MHz, DMSO-d_6) δ 13.12 (s, 1H), 10.45 (s, 1H), 8.62 – 8.56 (m, 1H), 8.13 (t, J = 2.0 Hz, 1H), 8.12 (d, J = 8.8 Hz, 1H), 7.94 – 7.88 (m, 1H), 7.87 (d, J = 1.7 Hz, 1H), 7.81 (td, J = 7.7, 1.8 Hz, 1H), 7.71 (d, J = 8.3 Hz, 1H), 7.67 (dd, J = 14.0, 4.8 Hz, 2H), 7.55 – 7.51 (m, 1H), 7.29 – 7.21 (m, 2H), 3.86 (s, 2H); ^{13}C NMR (126 MHz, DMSO-d_6) δ 169.04, 155.47, 149.99, 142.33, 142.20, 137.97, 137.34, 136.43, 135.64, 131.96, 129.41, 129.24, 126.85, 124.66, 124.45, 122.98, 122.85, 122.31, 121.47, 117.57, 115.19, 99.75, 42.42; LC/MS (ESI, m/z) 457.11 $[M + H]^+$.

(E)-1-(4-Chloro-3-(trifluoromethyl)phenyl)-3-(3-(2-(pyridin-2-yl)vinyl)-1H-indazol-6-yl)urea (10) To a solution of **37** (20 mg, 0.06 mmol) in DCM (20 mL) were added 4-chloro-3-(trifluoromethyl)phenyl isocyanate (13.8 mg, 0.06 mmol). The resulting mixture was stirred at room temperature for 8 h and then concentrated to dryness. The residue was diluted with DCM (1 mL) and CF_3COOH (0.5 mL). The reaction mixture was stirred at room temperature for 4 h and then the pH value was adjusted to 12 with saturated sodium bicarbonate. The mixture was extracted by EtOAc (50 mL) and washed with water (50 mL × 2) followed by brine (50 mL).

The organic layers were dried over sodium sulfate, filtered, concentrated and purified by silica gel column chromatography (eluting with 0−5% MeOH in DCM) to afford **10** as a yellow solid (17 mg, 62%). ^{1}H NMR (400 MHz, DMSO-d_6) δ 13.09 (s, 1H), 9.41 (s, 1H), 9.29 (s, 1H), 8.62 (s, 1H), 8.17 (s, 1H), 8.09 (d, J = 7.9 Hz, 1H), 7.98 (s, 1H), 7.92 (d, J = 16.5 Hz, 1H), 7.81 (d, J = 6.9 Hz, 1H), 7.73 – 7.59 (m, 3H), 7.54 (d, J = 16.4 Hz, 1H), 7.28 (s, 1H), 7.13 (d, J = 8.2 Hz, 1H); ^{13}C NMR (126 MHz, DMSO-d_6) δ 155.52, 153.06, 149.99, 142.70, 142.11, 139.87, 138.42, 137.32, 132.46, 129.15, 127.27, 124.69, 124.29, 123.60, 122.94, 122.82, 122.22, 121.42, 117.27, 117.00, 115.14, 98.69; LC/MS (ESI, m/z) 458.10 $[M + H]^+$.

(E)-N-(4-Chloro-3-(trifluoromethyl)phenyl)-N-(3-(2-(pyridin-2-yl)vinyl)-1H-indazol-6-yl)cyclopropane-1,1-dicarboxamide (11) Yield = 53%. ^{1}H NMR (400 MHz, DMSO-d_6) δ 13.22 (s, 1H), 10.45 (s, 1H), 10.25 (s, 1H), 8.63 (s, 1H), 8.29 (s, 1H), 8.15 (s, 1H), 8.11 (d, J = 8.3 Hz, 1H), 7.96 (d, J = 15.8 Hz, 2H), 7.88 (s, 1H), 7.75 (s, 1H), 7.68 (d, J = 8.9 Hz, 1H), 7.56 (d, J = 16.7 Hz, 1H), 7.39 – 7.30 (m, 2H), 1.51 (s, 4H); ^{13}C NMR (126 MHz, DMSO-d_6) δ 169.26, 168.28, 154.93, 148.96, 142.18, 141.92, 139.01, 138.36, 137.94, 132.35, 127.95, 127.03, 126.73, 126.71, 125.71, 125.54, 124.60, 124.35, 123.09, 122.22, 121.73, 121.04, 119.60, 119.55, 117.71, 116.35, 115.38, 101.14, 32.88, 15.85; LC/MS (ESI, m/z) 526.13 $[M + H]^+$.

N^1-(4-Chloro-3-(trifluoromethyl)phenyl)-N^3-(1H-indazol-6-yl)malonamide (12) Yield = 53%.^{1}H NMR (500 MHz, DMSO-d_6) δ 12.91 (s, 1H), 10.66 (s, 1H), 10.34 (s, 1H), 8.22 (s, 1H), 8.15 (s, 1H), 7.97 (s, 1H), 7.86 (d, J = 8.8 Hz, 1H), 7.73 – 7.64 (m, 2H), 7.09 (d, J = 8.6 Hz, 1H), 3.55 (s, 2H); ^{13}C NMR (126 MHz, DMSO-d_6) δ 166.67, 165.70, 140.76, 138.84, 137.49, 133.80, 132.71, 127.36, 124.34, 122.08, 121.22, 119.73, 118.17, 114.42, 99.41, 46.59. LC/MS (ESI, m/z) 397.07 $[M + H]^+$.

N^1-(4-Chloro-3-(trifluoromethyl)phenyl)-N^3-(3-methyl-1H-indazol-6-yl)malonamide (13) Yield = 46%. ^{1}H NMR (500 MHz, DMSO-d_6) δ 12.47 (s, 1H), 10.65 (s, 1H), 10.30 (s, 1H), 8.22 (d, J = 2.4 Hz, 1H), 8.05 (d, J = 1.0 Hz, 1H), 7.85 (dd, J = 8.8, 2.4 Hz, 1H), 7.69 (d, J = 8.8 Hz, 1H), 7.61 (d, J = 8.6 Hz, 1H), 7.06 (dd, J = 8.6, 1.6 Hz, 1H), 3.55 (s, 2H), 2.44 (s, 3H); ^{13}C NMR (126 MHz, DMSO-d_6) δ 166.69, 165.64, 141.67, 141.40, 138.84, 137.51, 132.70, 127.32, 124.33, 122.01, 120.64, 119.10, 118.12, 113.51, 99.39, 46.59, 12.11; LC/MS (ESI, m/z) 411.09 $[M + H]^+$.

N^1-(4-Chloro-3-(trifluoromethyl)phenyl)-N^3-(3-(1-methyl-1H-pyrazol-4-yl)-1H-indazol-6-yl)malonamide (14) Yield = 45%. ^{1}H NMR (400 MHz, DMSO-d_6) δ 12.81 (s, 1H), 10.80 (s, 1H), 10.47 (s, 1H), 8.33 (s, 1H), 8.23 (s, 1H), 8.13 (s, 1H), 7.96 (s, 2H), 7.87 (s, 1H), 7.71 (s, 1H), 7.15 (s, 1H), 3.92 (s, 3H), 3.56 (s, 2H); ^{13}C NMR (126 MHz, DMSO-d_6) δ 166.65, 165.73, 142.00, 138.90, 137.85, 137.73, 136.85, 132.69, 128.77, 127.16, 124.51, 124.35, 122.09, 121.19, 118.18, 116.96, 115.41, 114.38, 99.56, 46.64, 39.06; LC/MS (ESI, m/z) 477.11 $[M + H]^+$.

N^1-(4-Chloro-3-(trifluoromethyl)phenyl)-N^3-(3-(pyridin-3-yl)-1H-indazol-6-yl)malonamide (15) Yield = 50%. ^{1}H NMR (400 MHz, DMSO-d_6) δ 13.29 (s, 1H), 10.70 (s, 1H), 10.46 (s, 1H), 9.19 (s, 1H), 8.63 – 8.56 (m, 1H), 8.37 – 8.33 (m, 1H), 8.23 (s, 2H), 8.08 – 8.03 (m, 1H), 7.89 – 7.84 (m, 1H), 7.73 – 7.66 (m, 1H), 7.58 – 7.50 (m, 1H), 7.28 – 7.19 (m, 1H), 3.58 – 3.57 (m, 2H); ^{13}C NMR (126 MHz, DMSO-d_6) δ 166.73, 165.95, 158.80, 148.81, 147.47, 142.60, 140.73, 138.75, 137.82, 134.51, 132.68, 130.09, 127.15, 124.57, 124.36, 121.23, 118.77, 118.15, 116.97, 116.46, 115.48, 99.88, 46.10; LC/MS (ESI, m/z) 474.10 $[M + H]^+$.

N^1-(4-Chloro-3-(trifluoromethyl)phenyl)-N^3-(3-(6-methylpyridin-3-yl)-1H-indazol-6-yl)malonamide (16) Yield = 57%. ^{1}H NMR (400 MHz, DMSO-d_6) δ 13.21 (s, 1H), 10.68 (s,

1H), 10.43 (s, 1H), 9.05 (s, 1H), 8.23-8.21 (m, 3H), 8.01 (s, 1H), 7.86 (s, 1H), 7.71 (s, 1H), 7.41 (d, J = 8.1 Hz, 1H), 7.23 (s, 1H), 3.58 (s, 2H), 2.55 (s, 3H); LC/MS (ESI, m/z) 488.11 $[M + H]^+$.

N^1-(4-Chloro-3-(trifluoromethyl)phenyl)-N^3-(3-(5-(methylcarbamoyl)pyridin-3-yl)-1H-indazol-6-yl)malonamide (17) Yield = 39%. ^{1}H NMR (400 MHz, DMSO-d_6) δ 13.40 (s, 1H), 10.70 (s, 1H), 10.48 (s, 1H), 9.29 (s, 1H), 9.00 (s, 1H), 8.82 (s, 1H), 8.68 (s, 1H), 8.23 (s, 2H), 8.12 (s, 1H), 7.86 (s, 1H), 7.70 (s, 1H), 7.25 (s, 1H), 3.58 (s, 2H), 2.85 (s, 3H); LC/MS (ESI, m/z) 531.12 $[M + H]^+$.

N^1-(4-Chloro-3-(trifluoromethyl)phenyl)-N^3-(3-(3-fluorophenyl)-1H-indazol-6-yl)malonamide (18) Yield = 56%. ^{1}H NMR (400 MHz, DMSO-d_6) δ 13.25 (s, 1H), 10.71 (s, 1H), 10.47 (s, 1H), 8.23 (s, 2H), 8.05 (d, J = 7.2 Hz, 1H), 7.85 (s, 2H), 7.71 (s, 2H), 7.56 (s, 1H), 7.22 (s, 2H), 3.57 (s, 2H); ^{13}C NMR (126 MHz, DMSO-d_6) δ 166.63, 165.85, 163.97, 162.04, 142.65, 142.31, 138.84, 137.77, 136.54, 132.71, 131.42, 127.18, 124.35, 123.11, 121.40, 118.13, 116.85, 115.42, 114.78, 113.45, 113.27, 99.73, 46.62; LC/MS (ESI, m/z) 491.09 $[M + H]^+$.

N^1-(3-(3-Carbamoylphenyl)-1H-indazol-6-yl)-N^3-(4-chloro-3-(trifluoromethyl)phenyl)malonamide (**19**) Yield = 37%. ^{1}H NMR (400 MHz, DMSO-d_6) δ 13.20 (s, 1H), 10.73 (s, 1H), 10.48 (s, 1H), 8.43 (s, 1H), 8.23 (s, 2H), 8.14 (s, 2H), 8.04 (s, 1H), 7.88 (s, 1H), 7.71 (s, 1H), 7.59 (s, 1H), 7.48 (s, 1H), 7.17 – 7.16 (m, 2H), 3.59 (s, 2H); LC/MS (ESI, m/z) 516.11 $[M + H]^+$.

N^1-(4-Chloro-3-(trifluoromethyl)phenyl)-N^3-(3-(4-(methylcarbamoyl)phenyl)-1H-indazol-6-yl)malonamide (20) Yield = 45%. ^{1}H NMR (400 MHz, DMSO-d_6) δ 13.24 (s, 1H), 10.72 (s, 1H), 10.47 (s, 1H), 8.52 (s, 1H), 8.23 (s, 2H), 8.07 (s, 3H), 7.98 (s, 2H), 7.89 (s, 1H), 7.71 (s, 1H), 7.25 (s, 1H), 3.59 (s, 2H), 2.83 (s, 3H); LC/MS (ESI, m/z) 530.12 $[M + H]^+$.

N^1-(4-Chloro-3-(trifluoromethyl)phenyl)-N^3-(3-(4-(4-methylpiperazin-1-yl)phenyl)-1H-indazol-6-yl)malonamide (21) Yield = 41%. ^{1}H NMR (400 MHz, DMSO-d_6) δ 12.90 (s, 1H), 10.70 (s, 1H), 10.41 (s, 1H), 8.23 (s, 1H), 8.15 (s, 1H), 7.95 (d, J = 9.0 Hz, 1H), 7.83 (d, J = 8.4 Hz, 4H), 7.70 (d, J = 8.7 Hz, 1H), 7.16 (d, J = 8.4 Hz, 1H), 7.07 (d, J = 8.8 Hz, 2H), 3.50 (s, 2H), 2.35 (s, 3H); LC/MS (ESI, m/z) 572.19 $[M + H]^+$.

N^1-(4-Chloro-3-(trifluoromethyl)phenyl)-N^3-(3-(4-((4-methylpiperazin-1-yl)methyl)phenyl)-1H-indazol-6-yl)malonamide (22) Yield = 40%. ^{1}H NMR (400 MHz, DMSO-d_6) δ 13.09 (s, 1H), 10.75 (s, 1H), 10.46 (s, 1H), 8.24 (s, 1H), 8.19 (s, 1H), 8.01 (d, J = 8.5 Hz, 1H), 7.95 (d, J = 7.6 Hz, 2H), 7.88 (d, J = 7.0 Hz, 1H), 7.70 (d, J = 8.4 Hz, 1H), 7.44 (d, J = 7.3 Hz, 2H), 7.22 (d, J = 7.7 Hz, 1H), 3.58 (d, J = 6.8 Hz, 4H), 2.68 (s, 4H), 2.51 (s, 4H), 2.40 (s, 3H); LC/MS (ESI, m/z) 585.20 $[M + H]^+$.

(E)-N^1-Phenyl-N^3-(3-(2-(pyridin-2-yl)vinyl)-1H-indazol-6-yl)malonamide (23) Yield = 58%. ^{1}H NMR (400 MHz, DMSO-d_6) δ 13.16 (s, 1H), 10.42 (s, 1H), 10.22 (s, 1H), 8.61 (s, 1H), 8.20 (s, 1H), 8.14 (s, 1H), 7.92 (d, J = 16.5 Hz, 1H), 7.82 (s, 1H), 7.65-7.63 (m, 3H), 7.55 (d, J = 16.3 Hz, 1H), 7.32-7.30 (m, 4H), 7.08 (s, 1H), 3.55 (s, 2H); ^{13}C NMR (126 MHz, DMSO-d_6) δ 166.60, 165.80, 163.96, 163.84, 162.03, 161.91, 155.12, 149.42, 141.89, 137.88, 128.50, 123.09, 123.01, 121.47, 117.64, 115.20, 102.53, 102.29, 99.68, 99.01, 46.68; LC/MS (ESI, m/z) 398.16 $[M + H]^+$.

(E)-N^1-(3-Fluorophenyl)-N^3-(3-(2-(pyridin-2-yl)vinyl)-1H-indazol-6-yl)malonamide (24) Yield = 56%. ^{1}H NMR (500 MHz, DMSO-d_6) δ 13.16 (s, 1H), 10.44 (d, J = 9.1 Hz, 2H), 8.61 (d, J = 4.3 Hz, 1H), 8.20 (s, 1H), 8.14 (d, J = 8.7 Hz, 1H), 7.92 (d, J = 16.4 Hz, 1H), 7.81 (t, J = 7.6 Hz, 1H), 7.69 – 7.60 (m, 2H), 7.55 (d, J = 16.4 Hz, 1H), 7.36 (dt, J = 23.1, 7.9 Hz, 2H), 7.31 – 7.19 (m, 2H), 6.91 (t, J = 8.3 Hz, 1H), 3.53 (d, J = 29.4 Hz, 2H); ^{13}C NMR (126 MHz, DMSO-

d_6) δ 166.28, 166.03, 163.58, 161.66, 155.48, 150.00, 142.36, 142.22, 141.07, 137.89, 137.34, 130.99, 129.28, 124.65, 123.00, 122.86, 121.50, 117.61, 115.32, 110.46, 106.46, 99.73, 63.88, 46.61; LC/MS (ESI, m/z) 416.15 $[M + H]^+$.

(E)-N^1-(3-Chlorophenyl)-N^3-(3-(2-(pyridin-2-yl)vinyl)-1H-indazol-6-yl)malonamide (25) Yield = 48%. ^{1}H NMR (400 MHz, DMSO-d_6) δ 13.14 (s, 1H), 10.42 (s, 2H), 8.61 (s, 1H), 8.19 (s, 1H), 8.13 (s, 1H), 7.87 (dd, J = 33.5, 16.8 Hz, 3H), 7.66 (s, 1H), 7.59 – 7.43 (m, 2H), 7.37 (s, 1H), 7.27 (s, 2H), 7.15 (s, 1H), 3.55 (s, 2H) LC/MS (ESI, m/z) 432.12 $[M + H]^+$.

(E)-N^1-(3-Bromophenyl)-N^3-(3-(2-(pyridin-2-yl)vinyl)-1H-indazol-6-yl)malonamide (26) Yield = 51%. ^{1}H NMR (400 MHz, DMSO-d_6) δ 13.16 (s, 1H), 10.49 (s, 2H), 8.61 (s, 1H), 8.19 (s, 1H), 8.14 (s, 1H), 8.01 (s, 1H), 7.92 (d, J = 16.4 Hz, 1H), 7.82 (s, 1H), 7.67 (s, 1H), 7.53 (s, 2H), 7.29-7.27 (m, 3H), 3.57 (s, 2H); LC/MS (ESI, m/z) 476.7 $[M + H]^+$.

(E)-N^1-(3-(2-(Pyridin-2-yl)vinyl)-1H-indazol-6-yl)-N^3-(m-tolyl)malonamide (27) Yield = 52%. ^{1}H NMR (400 MHz, DMSO-d_6) δ 13.17 (s, 1H), 10.43 (s, 1H), 10.16 (s, 1H), 8.62 (s, 1H), 8.21 (s, 1H), 8.17 – 8.11 (m, 1H), 7.90 (s, 1H), 7.82 (s, 1H), 7.68 (s, 1H), 7.58 – 7.53 (m, 1H), 7.48 (s, 1H), 7.44 – 7.42 (m, 1H), 7.23 (s, 3H), 6.92 – 6.83 (m, 1H), 3.82 – 3.74 (m, 2H), 2.24 (s, 3H); LC/MS (ESI, m/z) 412.18 $[M + H]^+$.

(E)-N^1-(3-Methoxyphenyl)-N^3-(3-(2-(pyridin-2-yl)vinyl)-1H-indazol-6-yl)malonamide (28) Yield = 48%. ^{1}H NMR (400 MHz, DMSO-d_6) δ 13.15 (s, 1H), 10.44 (s, 1H), 10.24 (s, 1H), 8.61 (s, 1H), 8.20 (s, 1H), 8.13 (s, 1H), 7.92 (d, J = 16.2 Hz, 1H), 7.82 (s, 1H), 7.67 (s, 1H), 7.55 (d, J = 16.1 Hz, 1H), 7.34 (s, 1H), 7.25 (s, 2H), 7.17 (s, 1H), 6.67 (s, 1H), 3.75 (s, 3H), 3.54 (s, 2H); LC/MS (ESI, m/z) 428.17 $[M + H]^+$.

(E)-N^1-(3-(Dimethylamino)phenyl)-N^3-(3-(2-(pyridin-2-yl)vinyl)-1H-indazol-6-yl)malonamide (29) Yield = 55%. ^{1}H NMR (400 MHz, DMSO-d_6) δ 13.14 (s, 1H), 10.38 (s,

1H), 10.01 (s, 1H), 8.61 (s, 1H), 8.21 (s, 1H), 8.16 – 8.10 (m, 1H), 7.90 (s, 1H), 7.82 (s, 1H), 7.67 (s, 1H), 7.57 (s, 1H), 7.24 (s, 2H), 7.07 (s, 2H), 6.95 (s, 1H), 6.47 (s, 1H), 3.52 (s, 2H), 2.89 (s, 6H); ^{13}C NMR (126 MHz, DMSO-d_6) δ 166.35, 165.70, 155.48, 151.27, 150.00, 142.38, 142.21, 140.19, 137.96, 137.34, 129.57, 129.25, 124.67, 123.01, 122.85, 121.47, 117.56, 115.15, 108.41, 107.83, 103.63, 99.68, 46.64, 40.55; LC/MS (ESI, m/z) 441.21 $[M + H]^+$.

(E)-N^1-(3-(2-(Pyridin-2-yl)vinyl)-1H-indazol-6-yl)-N^3-(3-(trifluoromethyl)phenyl)malonamide (30) Yield = 47%. ^{1}H NMR (400 MHz, DMSO-d_6) δ 13.15 (s, 1H), 10.61 (s, 1H), 10.45 (s, 1H), 8.60 (s, 1H), 8.19 (s, 1H), 8.14 (s, 2H), 7.92 (d, J = 15.6 Hz, 1H), 7.81 (s, 2H), 7.66 (s, 1H), 7.55 (d, J = 15.9 Hz, 2H), 7.44 (s, 1H), 7.25 (s, 2H), 3.58 (s, 2H); ^{13}C NMR (126 MHz, DMSO-d_6) δ 166.52, 165.95, 155.48, 150.00, 142.35, 142.22, 140.16, 137.89, 137.34, 130.58, 129.84, 129.27, 125.64, 124.65, 123.11, 123.01, 122.85, 121.49, 120.24, 117.61, 115.58, 115.13, 99.73, 46.63; LC/MS (ESI, m/z) 466.15 $[M + H]^+$.

(E)-N^1-(3-(4-Methylpiperazin-1-yl)phenyl)-N^3-(3-(2-(pyridin-2-yl)vinyl)-1H-indazol-6-yl)malonamide (31) Yield = 46%. ^{1}H NMR (400 MHz, DMSO-d_6) δ 13.14 (s, 1H), 10.40 (s, 1H), 10.08 (s, 1H), 8.61 (s, 1H), 8.20 (s, 1H), 8.13 (s, 1H), 7.93 (d, J = 16.3 Hz, 1H), 7.81 (s, 1H), 7.67 (s, 1H), 7.55 (d, J = 15.4 Hz, 1H), 7.34-7.25 (m, 3H), 7.15 (s, 1H), 7.04 (s, 1H), 6.69 (s, 1H), 3.52 (s, 2H), 3.34 (s, 4H), 3.14 (s, 4H), 2.29 (s, 3H); LC/MS (ESI, m/z) 496.25 $[M + H]^+$.

(E)-N^1-(2-Fluorophenyl)-N^3-(3-(2-(pyridin-2-yl)vinyl)-1H-indazol-6-yl)malonamide (32) Yield = 50%. ^{1}H NMR (400 MHz, DMSO-d_6) δ 13.16 (s, 1H), 10.43 (s, 1H), 10.08 (s, 1H), 8.61 (s, 1H), 8.20 (s, 1H), 8.14 (s, 1H), 8.01 (s, 1H), 7.92 (d, J = 17.2 Hz, 1H), 7.82 (s, 1H), 7.67 (s, 1H), 7.55 (d, J = 16.9 Hz, 1H), 7.28-7.19 (m, 5H), 3.66 (s, 2H); ^{13}C NMR (126 MHz, DMSO-d_6) δ 166.43, 166.22, 155.48, 154.67, 152.83, 150.00, 142.36, 142.21, 137.85, 137.34, 129.27,

124.89, 124.65, 123.98, 123.01, 122.85, 121.49, 117.62, 116.00, 115.85, 115.16, 99.80; (ESI, m/z) 416.15 $[M + H]^+$.

(E)-N^1-(4-Fluorophenyl)-N^3-(3-(2-(pyridin-2-yl)vinyl)-1H-indazol-6-yl)malonamide (33) Yield = 47%. ^{1}H NMR (400 MHz, DMSO-d_6) δ 13.28 (s, 1H), 10.43 (s, 1H), 10.16 (s, 1H), 8.62 (s, 1H), 8.21 (s, 1H), 8.15 (s, 1H), 7.90 (s, 1H), 7.82 (s, 1H), 7.68 (s, 1H), 7.57 (s, 1H), 7.48 (s, 1H), 7.43 (s, 1H), 7.23 (s, 3H), 6.92 (s, 1H), 3.46 (s, 2H); (ESI, m/z) 416.15 $[M + H]^+$.

(E)-N^1-(3,5-Difluorophenyl)-N^3-(3-(2-(pyridin-2-yl)vinyl)-1H-indazol-6-yl)malonamide (34) Yield = 45%. ^{1}H NMR (400 MHz, DMSO-d_6) δ 13.19 (s, 1H), 10.65 (s, 1H), 10.46 (s, 1H), 8.62 (s, 1H), 8.19 (s, 1H), 8.14 (s, 1H), 7.94 (d, J = 15.5 Hz, 1H), 7.86 (s, 1H), 7.72 (s, 1H), 7.56 (d, J = 15.8 Hz, 1H), 7.35 (s, 3H), 7.23 (s, 1H), 6.96 (s, 1H), 3.56 (s, 2H); (ESI, m/z) 434.15 $[M + H]^+$.

(E)-N^1-(2,5-Difluorophenyl)-N^3-(3-(2-(pyridin-2-yl)vinyl)-1H-indazol-6-yl)malonamide (35) Yield = 46%. ^{1}H NMR (400 MHz, DMSO-d_6) δ 13.16 (s, 1H), 10.44 (s, 1H), 10.30 (s, 1H), 8.60 (s, 1H), 8.19 (s, 1H), 8.14 (s, 1H), 8.00 (s, 1H), 7.92 (d, J = 16.3 Hz, 1H), 7.81 (s, 1H), 7.66 (s, 1H), 7.55 (d, J = 16.3 Hz, 1H), 7.36 (s, 1H), 7.25 (d, J = 18.8 Hz, 2H), 7.00 (s, 1H), 3.69 (s, 2H); (ESI, m/z) 434.15 $[M + H]^+$.

(E)-N^1-(Perfluorophenyl)-N^3-(3-(2-(pyridin-2-yl)vinyl)-1H-indazol-6-yl)malonamide (36) Yield = 43%. ^{1}H NMR (400 MHz, DMSO-d_6) δ 13.16 (s, 1H), 10.49 (s, 1H),10.40 (s, 1H), 8.60 (s, 1H), 8.20 (s, 1H), 8.15 (s, 1H), 7.91 (d, J = 16.9 Hz, 1H), 7.81 (s, 1H), 7.66 (s, 1H), 7.55 (d, J = 16.2 Hz, 1H), 7.25 (d, J = 22.2 Hz, 2H), 3.63 (s, 2H); (ESI, m/z) 488.12 $[M + H]^+$.

Methyl (E)-3-oxo-3-((3-(2-(pyridin-2-yl)vinyl)-1-(tetrahydro-2H-pyran-2-yl)-1H-indazol-6-yl)amino)propanoate (38a) To a solution of **37** (500 mg, 1.56 mmol) in DMF (15 mL) were added methyl hydrogen malonate (240 mg, 1.88 mmol), HATU (770.6 mg, 2.03 mmol) and

DIEPA (402 mg, 3.12 mmol). The resulting mixture was stirred at room temperature for 2 h. Then it was diluted with EtOAc (100 mL) and washed with water (100 mL × 3) and brine (100 mL). The organic layers were dried over anhydrous sodium sulfate, filtered, concentrated and purified by silica gel column chromatography (eluting with 0−5% MeOH in DCM) to afford **38a** as a yellow solid (557 mg, 85%). Yield = 86%. ^{1}H NMR (400 MHz, DMSO-d_6) δ 10.49 (s, 1H), 8.62 (s, 1H), 8.22 (s, 1H), 8.15 (d, J = 8.5 Hz, 1H), 7.90 (d, J = 16.5 Hz, 1H), 7.82 (s, 1H), 7.69 (d, J = 7.3 Hz, 1H), 7.58 (d, J = 16.4 Hz, 1H), 7.31 (d, J = 8.5 Hz, 2H), 5.77 (d, J = 6.9 Hz, 1H), 3.92 (d, J = 10.0 Hz, 1H), 3.69 (s, 3H), 3.56 (s, 2H), 2.43 (d, J = 11.1 Hz, 1H), 2.03 (s, 2H), 1.80 (s, 1H), 1.61 (s, 2H); ^{13}C NMR (101 MHz, DMSO-d_6) δ 168.52, 164.87, 155.24, 150.03, 141.76, 141.44, 138.20, 137.37, 130.35, 123.78, 123.14, 123.06, 121.79, 119.04, 115.82, 100.14, 84.85, 67.07, 52.48, 44.07, 29.26, 25.29, 22.48; (ESI, m/z) 421.19 $[M + H]^+$.

Compounds **38b** and **45** were prepared following the synthetic procedure of compound **38a**.

Methyl (E)-1-((3-(2-(pyridin-2-yl)vinyl)-1-(tetrahydro-2H-pyran-2-yl)-1H-indazol-6-yl)carbamoyl)cyclopropane-1-carboxylate (**38b**) ^{1}H NMR (500 MHz, DMSO-d_6) δ 10.60 (s, 1H), 8.63 (s, 1H), 8.24 (s, 1H), 8.13 (d, J = 8.7 Hz, 1H), 7.92 (d, J = 16.4 Hz, 1H), 7.87 (t, J = 7.6 Hz, 1H), 7.76 (d, J = 7.8 Hz, 1H), 7.59 (d, J = 16.4 Hz, 1H), 7.40 (d, J = 8.8 Hz, 1H), 7.35 – 7.30 (m, 1H), 5.77 (d, J = 9.4 Hz, 1H), 3.93-39.1 (m, 1H), 3.77 – 3.67 (m, 4H), 2.47-2.37 (m, 1H), 2.11 – 1.96 (m, 2H), 1.80 (s, 1H), 1.58-1.48 (m, 2H), 1.52 – 1.46 (m, 2H), 1.45-1.42 (m, 2H); ^{13}C NMR (126 MHz, DMSO-d_6) δ 180.42, 172.33, 166.77, 154.91, 149.37, 141.66, 141.49, 138.47, 137.98, 129.64, 124.40, 123.22, 121.62, 118.93, 116.15, 100.21, 84.79, 67.10, 52.96, 30.55, 29.27, 25.29, 22.51, 16.86, 15.61; (ESI, m/z) 447.21 $[M + H]^+$.

(E)-3-oxo-3-((3-(2-(Pyridin-2-yl)vinyl)-1-(tetrahydro-2H-pyran-2-yl)-1H-indazol-6-yl)amino)propanoic acid (39a) To a solution of **38a** (328 mg, 0.78 mmol) in THF (15 mL) were

added LiOH (188 mg, 7.84 mmol) and water (15 mL). The reaction mixture was stirred at room temperature for 6 h under argon protection. The mixture was acidified with 1 N hydrochloric acid to pH = 3. The yellow precipitate was filtered and dried to provide **39a** (245 mg, 75%). ^{1}H NMR (400 MHz, DMSO-d_6) δ 12.75 (s, 1H), 10.46 (s, 1H), 8.62 (s, 1H), 8.24 (s, 1H), 8.14 (d, J = 8.5 Hz, 1H), 7.91 (d, J = 16.3 Hz, 1H), 7.83 (s, 1H), 7.71 (d, J = 7.2 Hz, 1H), 7.59 (d, J = 16.3 Hz, 1H), 7.33 (d, J = 9.3 Hz, 2H), 5.77 (d, J = 8.6 Hz, 1H), 3.92 (d, J = 9.7 Hz, 1H), 3.73 (s, 1H), 3.45 (s, 2H), 2.44 (d, J = 10.5 Hz, 1H), 2.03 (s, 2H), 1.79 (s, 1H), 1.60 (s, 2H); ^{13}C NMR (101 MHz, DMSO-d_6) δ 169.68, 165.44, 156.51, 155.09, 149.78, 141.70, 141.47, 138.37, 137.62, 130.03, 124.05, 123.17, 123.11, 121.72, 118.97, 115.86, 100.06, 84.87, 67.08, 44.59, 29.26, 25.28; (ESI, m/z) 418.18 $[M + H]^+$.

Compounds **39b** and **46** were prepared following the synthetic procedure of compound **39a**.

(E)-1-((3-(2-(Pyridin-2-yl)vinyl)-1-(tetrahydro-2H-pyran-2-yl)-1H-indazol-6-yl)carbamoyl)cyclopropane-1-carboxylic acid (39b) Yield = 74%. ^{1}H NMR (500 MHz, DMSO-d_6) δ 10.92 (s, 1H), 8.78 (t, J = 6.2 Hz, 1H), 8.56 – 8.45 (m, 2H), 8.40 – 8.34 (m, 1H), 8.30 (s, 1H), 8.24 (t, J = 6.7 Hz, 1H), 7.95 (t, J = 12.9 Hz, 1H), 7.82 (t, J = 6.4 Hz, 1H), 7.45 (d, J = 8.8 Hz, 1H), 5.85 (d, J = 9.7 Hz, 1H), 3.92 (d, J = 11.3 Hz, 1H), 3.79 – 3.72 (m, 1H), 2.45-2.39 (m, 1H), 2.10-2.02 (m, 2H), 1.87 – 1.75 (m, 1H), 1.65 – 1.56 (m, 2H), 1.53-1.48 (m, 4H); ^{13}C NMR (126 MHz, DMSO-d_6) δ 174.16, 167.60, 150.77, 145.24, 142.13, 141.62, 140.69, 138.54, 131.39, 125.08, 124.16, 121.44, 121.13, 118.97, 116.86, 100.47, 84.86, 67.11, 29.41, 29.23, 25.25, 22.39, 17.61; (ESI, m/z) 433.19 $[M + H]^+$.

6-Nitro-1-(tetrahydro-2H-pyran-2-yl)-1H-indazole (42a) To a solution of **41a** (0.50 g, 3 mmol) in anhydrous THF (10 mL) was added 3,4-dihydropyran (0.91 ml, 10 mmol) and methanesulfonic acid (0.03 g, 0.3 mmol) at 0 °C. The reaction mixture was stirred at 80 °C under

argon for 8 h and then cooled to room temperature before poured into saturated sodium bicarbonate (50 mL). The mixture was extracted by EtOAc (50 mL) and washed with water (50 mL × 2) followed by brine (50 mL). The organic layers were dried over sodium sulfate, filtered, concentrated and purified by silica gel column chromatography (eluting with 0−10% EtOAc in heptane) to afford **42a** as a white solid (621 mg, 81%). ^{1}H NMR (500 MHz, DMSO-d_6) δ 8.75 (s, 1H), 8.38 (s, 1H), 8.03 (q, J = 8.8 Hz, 2H), 6.12 (d, J = 9.1 Hz, 1H), 3.95 – 3.82 (m, 2H), 2.43-2.30 (m, 1H), 2.13 – 2.00 (m, 2H), 1.82-1.73 (m, 1H), 1.62-1.56 (m, 2H); ^{13}C NMR (126 MHz, DMSO-d_6) δ 145.54, 137.49, 133.65, 126.67, 121.75, 115.13, 106.53, 83.37, 65.93, 28.29, 24.16, 21.38.

Compound **42b** were prepared following the synthetic procedure of compound **42a**.

3-Methyl-6-nitro-1-(tetrahydro-2H-pyran-2-yl)-1H-indazole (42b) Yield = 74%. ^{1}H NMR (500 MHz, DMSO-d_6) δ 8.66 (s, 1H), 7.97 (s, 2H), 6.02 (dd, J = 9.6, 1.8 Hz, 1H), 3.87 (s, 2H), 2.51 (s, 1H), 2.42 – 2.33 (m, 1H), 2.05-1.94 (m, 2H), 1.79-1.70 (m, 1H), 1.65 – 1.56 (m, 2H), 1.52 – 1.41 (m, 2H); ^{13}C NMR (126 MHz, DMSO-D6) δ 145.66, 141.70, 138.31, 125.97, 121.09, 114.40, 106.26, 83.08, 66.00, 28.39, 24.18, 21.54, 11.00.

3-(1-Methyl-1H-pyrazol-4-yl)-6-nitro-1-(tetrahydro-2H-pyran-2-yl)-1H-indazole (42c) To a mixture of **40** (0.75 g, 2.0 mmol) and 1,4-dioxane/H_2O (20 mL, v/v, 5:1) were added 1-methyl-4-(4,4,5,5-tetramethyl-1,3,2-dioxaborolan-2-yl)-1H-pyrazole (0.50 g, 2.4 mmol), K_2CO_3 (0.83 g, 6.0 mmol) and $Pd(PPh_3)_4$ (0.23 g, 0.2 mmol). The reaction mixture was placed in an oil bath preheated to 90 °C and stirred at this temperature for 12 h under argon. Then the reaction mixture was cooled to rt before pouring into water (20 mL). The mixture was extracted by EtOAc (50 mL) and washed with water (50 mL) followed by brine (50 mL). The organic layers were dried over sodium sulfate, filtered, concentrated and purified by silica gel column chromatography

(eluting with 0−5% MeOH in DCM) to afford **42c** as a yellow solid (0.54 g, 83%). ^{1}H NMR (500 MHz, DMSO-d_6) δ 8.74 (s, 1H), 8.48 (s, 1H), 8.27 (d, J = 8.9 Hz, 1H), 8.05 (s, 1H), 8.02 (dd, J = 8.8, 1.5 Hz, 1H), 6.11 (d, J = 9.3 Hz, 1H), 3.95 (s, 3H), 3.94 – 3.78 (m, 2H), 2.52-2.41 (m, 1H), 2.11 – 1.98 (m, 2H), 1.84 – 1.73 (m, 1H), 1.61 (s, 2H); ^{13}C NMR (126 MHz, DMSO-d_6) δ 146.77, 139.65, 138.75, 137.19, 129.66, 124.66, 122.56, 116.08, 113.63, 107.64, 84.35, 67.11, 29.42, 25.19, 22.52; (ESI, m/z) 328.14 $[M + H]^+$.

Compound **42d-k** were prepared following the synthetic procedure of compound **42c**.

6-Nitro-3-(pyridin-3-yl)-1-(tetrahydro-2H-pyran-2-yl)-1H-indazole (42d) Yield = 76%. ^{1}H NMR (400 MHz, DMSO-d_6) δ 9.18 (s, 1H), 8.80 (s, 1H), 8.68 (s, 1H), 8.35 (s, 2H), 8.05 (s, 1H), 7.59 (s, 1H), 6.20 (s, 1H), 3.90 (s, 2H), 2.48 (s, 1H), 2.09 (s, 2H), 1.92 – 1.71 (m, 1H), 1.63 (s, 2H); ^{13}C NMR (100 MHz, DMSO-D6-d_6) δ 150.10, 148.17, 146.75, 141.59, 140.12, 134.95, 128.32, 124.74, 124.62, 122.75, 116.98, 108.05, 84.60, 67.02, 29.27, 25.15, 22.31; (ESI, m/z) 325.13 $[M + H]^+$.

3-(6-Methylpyridin-3-yl)-6-nitro-1-(tetrahydro-2H-pyran-2-yl)-1H-indazole (42e) Yield = 78%. ^{1}H NMR (400 MHz, DMSO-d_6) δ 9.03 (d, J = 17.4 Hz, 1H), 8.79 (d, J = 18.2 Hz, 1H), 8.25 (s, 1H), 8.03 (d, J = 9.5 Hz, 1H), 7.46 (s, 1H), 7.26 (s, 1H), 6.18 (s, 1H), 3.90 (s, 2H), 2.56 (d, J = 9.8 Hz, 4H), 2.06 (s, 2H), 1.79 (s, 1H), 1.62 (s, 2H); ^{13}C NMR (100 MHz, DMSO-d_6) δ 158.73, 147.41, 146.57, 141.70, 140.04, 135.07, 125.49, 124.68, 123.82, 122.69, 116.79, 107.92, 84.56, 67.05, 29.28, 25.17, 24.38, 22.37; (ESI, m/z) 339.15 $[M + H]^+$.

N-methyl-5-(6-nitro-1-(tetrahydro-2H-pyran-2-yl)-1H-indazol-3-yl)nicotinamide (42f) Yield = 74%. ^{1}H NMR (500 MHz, DMSO-d_6) δ 9.31 (s, 1H), 9.09 (s, 1H), 8.90 (s, 1H), 8.86 (s, 1H), 8.71 (s, 1H), 8.42 (s, 1H), 8.11 (d, J = 9.0 Hz, 1H), 6.25 (d, J = 9.2 Hz, 1H), 3.98 – 3.85 (m, 2H), 2.87 (s, 3H), 2.53-2.49 (m, 1H), 2.11-2.09 (m, 2H), 1.85-1.78(m, 1H), 1.64 (s, 2H); ^{13}C

NMR (126 MHz, DMSO-d_6) δ 165.10, 149.83, 148.52, 146.87, 140.98, 140.21, 133.45, 130.78, 128.14, 124.69, 122.89, 117.17, 108.15, 84.60, 67.13, 29.33, 26.75, 25.14, 22.37; (ESI, m/z) 382.15 $[M + H]^+$.

3-(3-Fluorophenyl)-6-nitro-1-(tetrahydro-2H-pyran-2-yl)-1H-indazole (42g) Yield = 83%. ^{1}H NMR (500 MHz, DMSO-d_6) δ 8.81 (s, 1H), 8.34 (d, J = 9.0 Hz, 1H), 8.06 (d, J = 9.0 Hz, 1H), 7.86 (d, J = 7.7 Hz, 1H), 7.76 (dd, J = 10.1, 1.2 Hz, 1H), 7.66 – 7.59 (m, 1H), 7.33 (td, J = 8.8, 2.3 Hz, 1H), 6.20 (d, J = 9.2 Hz, 1H), 3.97 – 3.82 (m, 2H), 2.50 – 2.42 (m, 1H), 2.08 (d, J = 9.9 Hz, 2H), 1.80 (td, J = 15.5, 8.5 Hz, 1H), 1.65 (d, J = 21.4 Hz, 2H); ^{13}C NMR (126 MHz, DMSO-d_6) δ 162.92, 160.97, 145.64, 141.86, 139.16, 133.51, 130.70, 123.54, 122.68, 115.92, 114.91, 112.92, 106.98, 83.46, 65.95, 28.20, 24.10, 21.28; (ESI, m/z) 342.13 $[M + H]^+$.

3-(6-Nitro-1-(tetrahydro-2H-pyran-2-yl)-1H-indazol-3-yl)benzamide (42h) Yield = 71%. ^{1}H NMR (500 MHz, DMSO-d_6) δ 8.83 (s, 1H), 8.45 (s, 1H), 8.35 (d, J = 9.0 Hz, 1H), 8.20 (s, 1H), 8.14 (d, J = 7.7 Hz, 1H), 8.10 (d, J = 8.9 Hz, 1H), 7.99 (d, J = 7.8 Hz, 1H), 7.66 (t, J = 7.7 Hz, 1H), 7.53 (s, 1H), 6.22 (d, J = 9.2 Hz, 1H), 3.90 (dt, J = 18.2, 11.4 Hz, 2H), 2.58 – 2.51 (m, 1H), 2.09-2.0 (m, 2H), 1.88 – 1.76 (m, 1H), 1.67-1.60 (m, 2H); ^{13}C NMR (126 MHz, DMSO-d_6) δ 168.05, 146.73, 143.75, 140.21, 135.69, 132.38, 130.36, 129.63, 128.19, 126.60, 124.73, 122.87, 116.90, 108.01, 84.51, 67.09, 29.36, 25.17, 22.42; (ESI, m/z) 367.14 $[M + H]^+$.

N-methyl-4-(6-nitro-1-(tetrahydro-2H-pyran-2-yl)-1H-indazol-3-yl)benzamide (**42i**) Yield = 69%. ^{1}H NMR (500 MHz, DMSO-d_6) δ 8.83 (s, 1H), 8.58 (d, J = 4.5 Hz, 1H), 8.38 (d, J = 9.0 Hz, 1H), 8.14 – 8.07 (m, 3H), 8.03 (d, J = 8.1 Hz, 2H), 6.23 (d, J = 8.9 Hz, 1H), 3.95 – 3.84 (m, 2H), 2.83 (s, 3H), 2.47 (s, 1H), 2.09 (d, J = 10.2 Hz, 2H), 1.91 – 1.76 (m, 1H), 1.65-1.89 (m, 2H); ^{13}C NMR (126 MHz, DMSO-d_6) δ 166.57, 146.72, 143.39, 140.26, 134.87, 134.70, 131.99,

129.28, 128.36, 127.36, 124.79, 122.93, 117.00, 108.06, 84.52, 67.06, 29.33, 26.78, 25.17, 22.38; (ESI, m/z) 381.16 $[M + H]^+$.

3-(4-(4-Methylpiperazin-1-yl)phenyl)-6-nitro-1-(tetrahydro-2H-pyran-2-yl)-1H-indazole (42j) Yield = 75%. ^{1}H NMR (400 MHz, DMSO-d_6) δ 8.73 (s, 1H), 8.21 (s, 1H), 8.01 (s, 1H), 7.81 (s, 2H), 7.07 (s, 2H), 6.12 (s, 1H), 3.89 (s, 2H), 3.40 (s, 1H), 3.22 (s, 4H), 2.47 (s, 4H), 2.24 (s, 3H), 2.05 (s, 2H), 1.78 (s, 1H), 1.61 (s, 2H); ^{13}C NMR (101 MHz, DMSO-d_6) δ 151.52, 146.50, 144.43, 140.09, 128.35, 124.76, 122.87, 122.38, 116.29, 115.63, 107.67, 84.43, 66.99, 54.94, 47.95, 46.19, 29.36, 25.22, 22.44; (ESI, m/z) 422.22 $[M + H]^+$.

3-(4-((4-Methylpiperazin-1-yl)methyl)phenyl)-6-nitro-1-(tetrahydro-2H-pyran-2-yl)-1H-indazole (**42k**) Yield = 71%. ^{1}H NMR (400 MHz, DMSO-d_6) δ 8.79 (s, 1H), 8.28 (s, 1H), 8.05 (s, 1H), 7.93 (s, 2H), 7.47 (s, 2H), 6.18 (s, 1H), 3.89 (s, 2H), 3.53 (s, 2H), 2.36 (s, 8H), 2.17 (s, 4H), 2.07 (s, 2H), 1.79 (s, 1H), 1.63 (s, 2H); ^{13}C NMR (101 MHz, DMSO-d_6) δ 146.62, 144.15, 140.16, 139.53, 130.98, 129.94, 127.47, 124.81, 122.86, 116.66, 107.90, 84.48, 66.98, 62.20, 55.14, 52.97, 46.10, 29.33, 25.19, 22.37; (ESI, m/z) 436.24 $[M + H]^+$.

1-(Tetrahydro-2H-pyran-2-yl)-1H-indazol-6-amine (43a) To a solution of **42a** (0.50 g, 2 mmol) in methanol (20 mL) was added 10% Pd/C (0.1 g) at room temperature under argon. Then the reaction mixture was stirred under a balloon of hydrogen for 20 h. The resulting mixture was filtered and washed with methanol. Evaporation of the filtrate provided the crude product, which was purified by silica gel flash chromatography (eluting with 0−30% EtOAc in heptane) to afford **43a** as a gray solid (0.35 g, 80%). ^{1}H NMR (500 MHz, DMSO-d_6) δ 7.74 (s, 1H), 7.36 (d, J = 8.5 Hz, 1H), 6.61 (s, 1H), 6.53 (d, J = 8.6 Hz, 1H), 5.53 (dd, J = 9.5, 1.9 Hz, 1H), 5.36 (s, 2H), 3.87 (d, J = 11.2 Hz, 1H), 3.69 – 3.55 (m, 1H), 2.41-2.33 (m, 1H), 2.01 (dd, J = 9.2, 4.0 Hz, 1H), 1.91-1.88 (m, 1H), 1.77 – 1.65 (m, 1H), 1.59 – 1.52 (m, 2H); ^{13}C NMR (126 MHz, DMSO-

d_6) δ 148.57, 141.93, 133.64, 121.43, 116.87, 113.15, 91.30, 84.49, 66.87, 29.29, 25.37, 22.78; (ESI, m/z) 218.13 $[M + H]^+$.

Compound **43b-k** were prepared following the synthetic procedure of compound **42c**.

3-Methyl-1-(tetrahydro-2H-pyran-2-yl)-1H-indazol-6-amine (43b) Yield = 70%. ^{1}H NMR (500 MHz, DMSO-d_6) δ 7.30 (d, J = 8.5 Hz, 1H), 6.54 (d, J = 4.9 Hz, 1H), 6.49 (d, J = 8.5 Hz, 1H), 5.50 – 5.38 (m, 1H), 5.31 (s, 2H), 3.87 (d, J = 11.1 Hz, 1H), 3.72 – 3.59 (m, 1H), 2.40 – 2.30 (m, 4H), 1.99 (dd, J = 9.5, 3.5 Hz, 1H), 1.84-1.81 (m, 1H), 1.77 – 1.66 (m, 1H), 1.57 – 1.47 (m, 2H); ^{13}C NMR (126 MHz, DMSO-d_6) δ 148.62, 142.83, 141.32, 120.85, 116.43, 112.24, 91.32, 84.27, 66.94, 29.40, 25.40, 22.96, 12.11; (ESI, m/z) 232.15 $[M + H]^+$.

3-(1-Methyl-1H-pyrazol-4-yl)-1-(tetrahydro-2H-pyran-2-yl)-1H-indazol-6-amine (43c) Yield = 69%. ^{1}H NMR (400 MHz, DMSO-d_6) δ 8.28 (s, 1H), 7.91 (s, 1H), 7.72 – 7.66 (m, 1H), 7.64 (d, J = 7.8 Hz, 1H), 7.59 ((d, J = 7.8 Hz, 1H), 6.74 (s, 2H), 5.70 – 5.48 (m, 1H), 4.71 (s, 1H), 3.86 (s, 1H), 3.65 (s, 1H), 2.43 (s, 1H), 1.99 (s, 1H), 1.90 (s, 1H), 1.71 (s, 2H), 1.54 (s, 3H); ^{13}C NMR (100 MHz, DMSO-d_6) δ 136.92, 132.52, 132.01, 131.91, 129.29, 129.18, 128.91, 115.41, 114.27, 112.70, 83.84, 67.05, 39.57, 29.51, 25.29, 23.04; (ESI, m/z) 298.17 $[M + H]^+$.

3-(Pyridin-3-yl)-1-(tetrahydro-2H-pyran-2-yl)-1H-indazol-6-amine (43d) Yield = 72%. ^{1}H NMR (500 MHz, DMSO-d_6) δ 9.10 (d, J = 1.6 Hz, 1H), 8.59 (d, J = 4.7 Hz, 1H), 8.26 (d, J = 7.9 Hz, 1H), 7.71 (s, 1H), 7.51 (dd, J = 7.8, 4.8 Hz, 1H), 6.68 (s, 1H), 6.66 (d, J = 8.7 Hz, 1H), 5.64 (dd, J = 9.4, 1.9 Hz, 1H), 5.52 (s, 2H), 3.92 (d, J = 11.4 Hz, 1H), 3.80 – 3.61 (m, 1H), 2.48 – 2.40 (m, 1H), 2.12 – 2.02 (m, 1H), 1.98-.192 (m, 1H), 1.82 – 1.70 (m, 1H), 1.64-1.55 (m, 2H); ^{13}C NMR (126 MHz, DMSO-d_6) δ 149.09, 148.89, 147.86, 143.57, 140.42, 134.34, 130.01, 124.42, 121.47, 114.23, 114.02, 91.47, 84.65, 66.98, 29.22, 25.32, 22.68; (ESI, m/z) 295.16 $[M + H]^+$.

3-(6-Methylpyridin-3-yl)-1-(tetrahydro-2H-pyran-2-yl)-1H-indazol-6-amine (**43e**) Yield = 74%. ^{1}H NMR (400 MHz, DMSO-d_6) δ 9.00 (d, J = 7.2 Hz, 1H), 8.17 (d, J = 7.9 Hz, 1H), 7.71 (t, J = 7.5 Hz, 1H), 7.36 (t, J = 7.7 Hz, 1H), 6.79 – 6.58 (m, 2H), 5.77 (s, 2H), 5.64 (d, J = 8.9 Hz, 1H), 3.92 (s, 1H), 3.70 (s, 1H), 2.53 (s, 2H), 2.46 (s, 1H), 2.19 – 1.79 (m, 2H), 1.74 (s, 1H), 1.58 (s, 3H); ^{13}C NMR (100 MHz, DMSO-d_6) δ 157.46, 148.81, 147.07, 143.53, 140.61, 134.72, 127.25, 123.69, 121.49, 114.09, 91.54, 84.66, 67.01, 55.38, 29.26, 25.33, 24.26, 22.73; (ESI, m/z) 309.17 $[M + H]^+$.

5-(6-Amino-1-(tetrahydro-2H-pyran-2-yl)-1H-indazol-3-yl)-N-methylnicotinamide (43f) Yield = 65%. ^{1}H NMR (500 MHz, DMSO-d_6) δ 9.26 (s, 1H), 9.04 (s, 1H), 8.90 (s, 1H), 8.67 (s, 1H), 8.01 (d, J = 8.7 Hz, 1H), 7.17 (s, 1H), 6.96 (d, J = 8.7 Hz, 1H), 5.80 (t, J = 11.3 Hz, 1H), 3.93 (d, J = 11.3 Hz, 1H), 3.79 – 3.70 (m, 1H), 2.86 (d, J = 4.4 Hz, 3H), 2.44 (s, 1H), 2.06 (dd, J = 24.0, 8.9 Hz, 2H), 1.88 – 1.74 (m, 1H), 1.62 (s, 2H); ^{13}C NMR (126 MHz, DMSO-d_6) δ 165.25, 149.40, 147.66, 142.56, 139.96, 133.14, 130.75, 129.43, 122.15, 116.77, 116.06, 97.13, 84.90, 67.06, 29.24, 26.75, 25.42, 25.25, 22.53; (ESI, m/z) 352.18 $[M + H]^+$.

3-(3-Fluorophenyl)-1-(tetrahydro-2H-pyran-2-yl)-1H-indazol-6-amine (43g) Yield = 76%. ^{1}H NMR (500 MHz, DMSO-d_6) δ 7.76 (t, J = 9.6 Hz, 1H), 7.70 (t, J = 13.7 Hz, 1H), 7.64 (d, J = 10.4 Hz, 1H), 7.57 – 7.49 (m, 1H), 7.25 – 7.17 (m, 1H), 6.67-6.65 (m, 2H), 5.63 (d, J = 9.2 Hz, 1H), 5.50 (s, 2H), 3.91 (d, J = 11.3 Hz, 1H), 3.78 – 3.64 (m, 1H), 2.49-2.41 (m, 1H), 2.13 – 2.01 (m, 1H), 1.98-1.95 (m, 1H), 1.80-1.71 (m, 1H), 1.63-1.55 (m, 2H); ^{13}C NMR (126 MHz, DMSO-d_6) δ 162.66, 160.77, 147.92, 142.49, 140.85, 135.36, 130.18, 122.05, 120.09, 113.88, 113.09, 112.84, 112.23, 90.42, 83.52, 65.87, 28.14, 24.26, 21.61; (ESI, m/z) 312.15 $[M + H]^+$.

3-(6-Amino-1-(tetrahydro-2H-pyran-2-yl)-1H-indazol-3-yl)benzamide (**43h**) Yield = 65%. ^{1}H NMR (500 MHz, DMSO-d_6) δ 8.36 (s, 1H), 8.13 (s, 1H), 8.04 (d, J = 7.6 Hz, 1H), 7.88 (d, J

= 7.7 Hz, 1H), 7.73 (d, *J* = 8.6 Hz, 1H), 7.57 (t, *J* = 7.7 Hz, 1H), 7.45 (s, 1H), 6.66 (d, *J* = 10.9 Hz, 2H), 5.63 (d, *J* = 9.5 Hz, 1H), 5.49 (s, 2H), 3.94-3.91 (m, 1H), 3.74 – 3.66 (m, 1H), 2.48-2.42 (m, 1H), 2.10 – 1.94 (m, 2H), 1.81 – 1.67 (m, 1H), 1.62-1.55 (m, 2H); (ESI, m/z) 337.17 $[M + H]^+$.

4-(6-Amino-1-(tetrahydro-2H-pyran-2-yl)-1H-indazol-3-yl)-N-methylbenzamide (**43i**) Yield = 69%. ^{1}H NMR (500 MHz, DMSO-d_6) δ 8.50 (s, 1H), 8.01 – 7.99 (m, 2H), 7.95 (d, *J* = 8.0 Hz, 2H), 7.76 (dd, *J* = 8.7, 3.7 Hz, 1H), 6.67 (d, *J* = 11.2 Hz, 2H), 5.63 (d, *J* = 9.4 Hz, 1H), 5.50 (s, 2H), 3.92 (d, *J* = 11.3 Hz, 1H), 3.74 – 3.66 (m, 1H), 2.82 (d, *J* = 3.4 Hz, 2H), 2.44 (dd, *J* = 17.5, 8.2 Hz, 1H), 2.07 – 1.94 (m, 2H), 1.79 – 1.73 (m, 1H), 1.62-1.57 (m, 2H); ^{13}C NMR (126 MHz, DMSO-d_6) δ 166.80, 148.75, 143.65, 142.25, 136.64, 133.85, 131.99, 129.28, 128.06, 126.78, 121.67, 114.11, 84.62, 67.00, 29.26, 26.75, 25.34, 22.72; (ESI, m/z) 351.18 $[M + H]^+$.

3-(4-(4-Methylpiperazin-1-yl)phenyl)-1-(tetrahydro-2H-pyran-2-yl)-1H-indazol-6-amine (**43j**) Yield = 68%. ^{1}H NMR (400 MHz, DMSO-d_6) δ 7.76 (s, 2H), 7.65 (s, 1H), 7.02 (s, 2H), 6.64 (s, 2H), 5.57 (s, 1H), 5.42 (s, 2H), 3.91 (s, 1H), 3.68 (s, 1H), 3.37 (s, 1H), 3.18 (s, 4H), 2.46 (s, 4H), 2.23 (s, 3H), 2.00 (d, *J* = 37.4 Hz, 2H), 1.74 (s, 1H), 1.57 (s, 2H); ^{13}C NMR (101 MHz, DMSO-d_6) δ 150.88, 148.47, 143.52, 143.34, 127.91, 124.65, 121.75, 115.62, 114.21, 113.39, 91.58, 84.57, 66.94, 55.04, 48.26, 46.25, 29.33, 25.40, 22.83; (ESI, m/z) 392.25 $[M + H]^+$.

3-(4-((4-Methylpiperazin-1-yl)methyl)phenyl)-1-(tetrahydro-2H-pyran-2-yl)-1H-indazol-6-amine (**43k**) Yield = 70%. ^{1}H NMR (500 MHz, DMSO-d_6) δ 7.88 (d, *J* = 7.8 Hz, 2H), 7.72 (d, *J* = 8.7 Hz, 1H), 7.43 (d, *J* = 7.9 Hz, 2H), 6.69 (s, 1H), 6.66 (d, *J* = 8.8 Hz, 1H), 5.64 (d, *J* = 8.0 Hz, 1H), 5.49 (s, 2H), 3.95-3.93 (m, 1H), 3.78 – 3.68 (m, 1H), 3.53 (s, 2H), 2.51 – 2.36 (m, 9H), 2.20 (s, 3H), 2.12 – 2.03 (m, 1H), 2.01 – 1.95 (m, 1H), 1.83 – 1.70 (m, 1H), 1.62 (s, 2H); ^{13}C NMR (126 MHz, DMSO-d_6) δ 148.62, 143.56, 143.06, 138.26, 134.49, 132.86, 129.67, 127.00,

121.67, 114.13, 113.75, 84.55, 66.93, 62.34, 55.18, 53.02, 46.17, 29.28, 25.14, 22.75;Yield = 70%; (ESI, m/z) 406.26 $[M + H]^+$.

Methyl 3-((4-chloro-3-(trifluoromethyl)phenyl)amino)-3-oxopropanoate (45) Yield = 83%. ^{1}H NMR (500 MHz, DMSO-d_6) δ 10.65 (s, 1H), 8.16 (d, J = 1.6 Hz, 1H), 7.81 (d, J = 8.7 Hz, 1H), 7.68 (d, J = 8.8 Hz, 1H), 3.67 (s, 3H), 3.52 (s, 2H); ^{13}C NMR (126 MHz, DMSO-d_6) δ 168.22, 165.23, 138.66, 132.73, 127.38, 124.72, 124.35, 122.04, 118.16, 118.12, 52.54, 43.96; (ESI, m/z) 296.03 $[M + H]^+$.

3-((4-Chloro-3-(trifluoromethyl)phenyl)amino)-3-oxopropanoic acid (46) Yield = 74%.^{1}H NMR (500 MHz, DMSO-d_6) δ 11.29 (s, 1H), 8.23 (d, J = 1.8 Hz, 1H), 7.84 (dd, J = 8.7, 1.6 Hz, 1H), 7.63 (d, J = 8.8 Hz, 1H), 3.29 (s, 2H); ^{13}C NMR (126 MHz, DMSO-d_6) δ 170.01, 167.36, 139.11, 132.50, 127.01, 124.27, 124.17, 124.05, 122.10, 117.95, 45.52; (ESI, m/z) 297.04 $[M + H]^+$.

Biochemical Kinase Assay. The inhibitory activities of **24** against c-KIT and c-KIT T670I were determined by the ADP-Glo assay. The optimized enzyme concentrations were chosen as follows: c-KIT 20 ng/μL, c-KIT T670I 15 ng/μL. In all cases, 2.5 μL samples of kinase was incubated with **24** for 60 min at room temperature in reaction buffer followed by addition of 2.5 μL ATP/substrate mixture. The ATP concentration was chosen as follows: 50 μM ATP for c-KIT or c-KIT T670I. The assay was conducted for 1 h at 37 °C before addition of 5 μL ADP-Glo reagent and incubation for 40 min at room temperature. 10 μL Kinase detection reagent was added and incubated for 30 min at room temperature before the luminescence signal was read with an envision Perkin Elmer plate reader (Envision, PE, USA), and then the dose–response curve was fitted using Prism 7.0 (GraphPad Software Inc., San Diego, CA). The biochemical tests of other targets were provided by Invitrogen (Carlsbad, CA, USA).

Imatinib and ponatinib were purchased from MedChem Express (Shanghai, China).

Cell Lines, Antibodies and Chemicals. The human GIST-T1 cell line was purchased from Cosmo Bio Co., Ltd. (Tokyo, Japan). GIST-882 and GIST-48B cell lines were kindly provided by the group of Professor Jonathan A. Fletcher, Brigham and Women's Hospital in Boston, USA. GIST-T1-T670I and TEL-isogenic BaF3 cell lines were established in our lab. GIST-5R cell line was kindly provided by prof. Brian Rubin, Department of Molecular Genetics, Lerner Research Institute, and Department of Anatomic Pathology and Taussing Cancer Center, Cleveland Clinic, Cleveland, OH 44195. GIST-T1, GIST-T1-T670I and GIST-5R cell lines were maintained in DMEM (Corning, USA) supplemented with 10% FBS, 1% penicillin/streptomycin. GIST882 and GIST-8B cell lines were maintained in IMEM (Gibco, USA) supplemented with 10% FBS, 1% penicillin/streptomycin. Isogenic BaF3 cells lines were cultured in RPMI 1640 media (Corning, USA) with 10% fetal bovine serum (FBS) and supplemented with 2% L-glutamine and 1% penicillin/streptomycin. All cell lines were maintained in culture media at 37 °C with 5% CO_2.

The following antibodies were purchased from Cell Signaling Technology (Danvers, MA): AKT (pan) (C67E7) rabbit mAb (no. 4691), Phospho-AKT (Thr308) (244F9) rabbit mAb (no. 4056), Phospho-AKT (Ser473) (D9E) XP rabbit mAb (no. 4060), GAPDH (D16H11) XP rabbit mAb, PARP (46D11) rabbit mAb (no. 9532), caspase-3 (8G10) rabbit mAb (no. 9665), Phospho-p44/42 MAPK (ERK1/2) (Thr202/Tyr204) (197G2) rabbit mAb (no. 4377), p44/42 MAPK (ERK1/2) (137F5) rabbit mAb (no. 4695), c-KIT (Ab81) mouse mAb (no. 3308), Phospho-c-KIT (Tyr703) (D12E12) rabbit mAb (no. 3073), Phospho-c-Kit (Tyr719) antibody (no. 3391), Phospho-anti-c-Kit (pY823) rabbit mAb (no. 77522), PhosphoSTAT3 (Tyr705) (D3A7) XP rabbit mAb (Biotinylated) (no. 4093), STAT3 (D3Z2G) rabbit mAb no. 12640, Phospho-S6 ribosomal protein (Ser235/236) antibody (no. 2211), S6 ribosomal protein (5G10) rabbit mAb

(no. 2217).

Generation of GIST-T1-T670I Cell Line using CRISPR/Cas9 System. SgRNA targeting the genomic region surrounding T670 site of KIT gene was designed and synthesized. Annealed sgRNA oligos were inserted into pSpCas9(BB)-2A-Puro (PX459) V2.0 vector (Addgene, Cambridge, MA, USA) and transfected into GIST-T1 cells together with a 90-nt oligo containing T670I mutation as HDR template by Lipofectamine 3000 (Invitrogen, Carlsbad, CA, USA). Antibiotic selection with puromycin was performed 2 days after transfection and then cells were diluted and cultured in 96-well plates with only one cell per well for 3 weeks. Correctly edited T670I knock-in cell clones were then confirmed by Sanger sequencing at targeted genomic region.

General Procedure for Antiproliferation Assays. For the non-adherent cells, a density of 1.5 to 5 × 10^4 cells/mL cells were mixed with various concentrations of compounds, then 100 μL suspension was added to each well and then incubated at 37 °C with 5% CO_2 for 72 h. For the adherent cells, a density of 1.5 to 5 × 10^4 cells/mL cells were added to 96-well plate, incubated at 37 °C with 5% CO_2 overnight. The next day the supernatant were changed with fresh medium containing different various concentrations of compounds and then incubated for 72 h. Cell viability was determined using CCK-8 KIT (MedChemExpress, China) according to the instruction manual. The absorbance was measured in a microplate reader (iMARK, Bio-Rad, USA) at 450 nm. Data were normalized to control group (DMSO). GI_{50} values were calculated using Prism 7.0 (GraphPad Software, San Diego, CA).

c-KIT Protein Purification. The sequences encoding c-KIT wt and c-KIT T670I residues 544−935 with a Histag were cloned into baculovirus expression vector pFASTHTA. The proteins were expressed by infecting SF9 cells with high titer viral stocks for 48 h. Cells were

harvested and lysed in 25 mM Tris pH 7.4, 250 mM NaCl and 1 mM PMSF. The supernatant was loaded to Ni-NTA column (QIAGEN, 1018244). Then the proteins were step-eluted with the same buffer with 250 mM imidazole. The eluted proteins were loaded on a Superdex-200 column equilibrated in 25 mM Tris (pH 7.4), 250 mM NaCl, 1 mM DTT, and 1 mM EDTA. Peak fractions were concentrated to 2 mg/mL and flash-frozen.

Signaling Pathway Study. GIST-T1, GIST-T1-T670I and GIST-5R cells were cultured in 10% FBS-containing DMEM medium. The serially diluted compound **24** was added to cells for 1 h. The cells were collected and lysed. The cell lysates were analyzed by Western blotting. Western blotting was performed by standard methods, as previously described.

Apoptosis Effect Examination. GIST-T1, GIST-T1-T670I and GIST-5R cells were cultured in 10% FBS-containing DMEM medium. The serially diluted compound **24** was added to cells for 24 h. Then, apoptosis of GIST-T1, GIST-T1-T670I and GIST-5R cells was detected by Western blot using PARP and GAPDH antibodies (Cell Signaling Technology).

Rodent Pharmacokinetics. The study protocol was approved by the animal ethics committee of Hefei Institutes of Physical Science, Chinese Academy of Sciences (Hefei, China). The male Sprague–Dawley rats (190-210 g) were provided by laboratory animal center of Anhui Medical University (Hefei, China). The animals were housed in an air-conditioned animal room at a temperature of 23 ± 2 °C and a relative humidity of 50 ± 10% and allowed free access to tap water and lab. The rats were acclimatized to the facilities for one week and then fasted for 12 h with free access to water prior to the experiment. The rats were randomly and equally divided into two groups for the pharmacokinetic study of the compound. One group was injected with *i.v.* formulation at a dose of 1 mg/kg. The other group was treated by oral administration of *p.o.* formulation at doses of 10 mg/kg. The *i.v.* formulation for rats was consisted of 5 mg compound

dissolved in 0.5 mL of dimethyl sulfoxide and 4.5 mL of 5% glucose water. The *p.o.* formulation for rats was made with 50 mg compound dissolved in 0.5 mL of dimethyl sulfoxide and 4.5 mL of 5% glucose water. About 300 μL of blood samples were collected into heparinized tubes at 2, 5, 15, 30, 60, 120, 240, 360, 540 and 720 min after intravenous injection of compound **24** and at 5, 15, 30, 60, 90, 120, 240, 360, 540 and 720 min after oral administration of compound **24**. 100 μL of plasma was harvested by centrifuging the blood sample at 4 °C and 5000 rpm for 3 min, and then stored at −80 °C until analysis. An aliquot of 100 μL of each plasma sample was mixed with 20 μL of internal standard working solution (200 ng/mL of caffeine). Methanol (400 μL) was then added for precipitation. After vortexing for 5 min and centrifuging at 14,000 rpm for 10 min, 5 μL of the supernatant was injected for LC-MS/MS analysis. The pharmacokinetic parameters were analyzed through noncompartment model using WinNonlin 6.1 software (Pharsight Corporation, Mountain View, USA). The oral bioavailability (F) is calculated according to the following equation: $F = AUC_{0-\infty}$ (oral) / $AUC_{0-\infty}$ (*iv*) × dose (*iv*) / dose (oral) ×100%.

GIST-5R Xenograft Model. Five-week old female nu/nu mice were purchased from the Nanjing Biomedical Research Institute of Nanjing University (Nanjing, China). All animals were maintained in the Animal Center of Hefei Institutes of Physical Science, Chinese Academy of Sciences according to the Guide for the Care and Use of Laboratory Animals (National Research Council [US] Committee). All the experimental protocols were approved by the Hefei Institutes of Physical Science ethics committee, Chinese Academy of Sciences (approval no. HFCASDWLL20160512). All efforts were made to minimize animal suffering. To obtain orthotopic xenograft of human mammary tumor in the mice, cells were harvested during exponential growth. One million GIST-5R cells in PBS were suspended in a 1:1 mixture with

Matrigel (BD Biosciences) and injected into the subcutaneous space on the right flank of nu/nu mice. Daily *p.o.* administration was initiated when GIST-5R tumors had reached a size of 200−400 mm^3. Animals were then randomized into treatment groups of 4 mice each for efficacy studies. Compound **24** was delivered in a HKI suspension (0.5% methocellulose/0.4% Tween80 in ddH_2O) by *p.o.* (QD). A range of doses of **24** or its vehicle was administered, as indicated in the Figure **9** legend. Body weight and tumor growth were measured daily after **24** treatment. Tumor volumes were calculated as follows: tumor volume (mm^3) = $[(W^2 \times L)/2]$ in which width (W) is defined as the smaller of the two measurements and length (L) is defined as the larger of the two measurements.

Molecular Modeling. All calculations were performed using the Schrödinger Suite. The DFG-out c-KIT complex (PDB ID: 1T46) was used for docking studies. The crystal structure was prepared using the Protein Preparation Wizard and the T670I mutant was modeled in situ within Maestro. The ligand structures were built in Maestro and prepared for docking using LigPrep (LigPrep 3.4, Schrödinger, LLC, New York, NY) and further docked into the receptor by the IFD protocol (Induced Fit Docking protocol, Schrödinger, LLC, New York, NY).

ASSOCIATE CONTENT

Supporting Information

The supporting information is available free of charge on the ACS Publication website at DOI:XXXXXX.

Supplementary Table 1 listing the DiscoverX's KINOMEscan selectivity profiling data of **24**.

Supplementary Figure 1 listing the pharmacodynamic evaluation of **24** in the GIST-5R xenograft mouse model.

Molecular formula strings (CSV)

Docking poses for **6**, **7** and **24** with c-KIT T670I and docking pose for **24** with c-KIT wt (PDB)

AUTHOR INFORMATION

Corresponding Authors

*For J.L.: phone, 86-551-65593186; E-mail, jingliu@hmfl.ac.cn.

*For Q.L.: phone, 86-551-65595161; E-mail, qsliu97@hmfl.ac.cn.

Author Contributions

The manuscript was written through contributions of all authors. All authors have given approval to the final version of the manuscript. X.L., B.W., C.C. and A.W. contributed equally to this work.

Notes

The authors declare no competing financial interest.

AKNOWLEDGMENTS

This work was supported by the National Natural Science Foundation of China (Grants 81603123, 81803366, 21708044, 81673469, 81773777, 81872748), the "Personalized Medicines-Molecular Signature-Based Drug Discovery and Development", Strategic Priority Research Program of the Chinese Academy of Sciences (Grant XDA12020224), the China Postdoctoral Science Foundation (Grants 2018T110634, 2018M630720), the Natural Science Foundation of Anhui Province (Grants 1808085MH268), the Major Science and Technology Program of Anhui Province (Grant 18030801116), the Key Research and Development Program of Anhui Province (Grant 1704a0802140), the Key Technology Research and Development Program of Hefei (Grant ZR201711290017) and the Frontier Science Key Research Program of

CAS (Grant QYZDB-SSW-SLH037). We are also grateful for the National Program for Support of Top-Notch Young Professionals for J.L. and the support of Hefei leading talent for F.Z..

ABBREVIATIONS

GISTs, gastrointestinal stromal tumors; PDGFR, platelet-derived growth factor receptor; CSF1R, colony stimulating factor 1 receptor; JM, juxtamembrane domain; RCC, renal cell carcinoma; TKD, tyrosine kinase domain; THP, tetrahydropyranyl; DIPEA, *N*,*N*-diisopropylethylamine; HATU, 1-[Bis(dimethylamino)methylene]-1H-1,2,3-triazolo[4,5-b]pyridinium 3-oxid hexafluorophosphate.

REFERENCES

[1] Zhao, X.; Yue, C. Gastrointestinal Stromal Tumor, *J. Gastrointest. Oncol.* **2012**, *3*, 189-208.

[2] Hirota, S.; Isozaki, K.; Moriyama, Y.; Hashimoto, K.; Nishida, T.; Ishiguro, S.; Kawano, K.; Hanada, M.; Kurata, A.; Takeda, M.; Muhammad Tunio, G.; Matsuzawa, Y.; Kanakura, Y.; Shinomura, Y.; Kitamura, Y. Gain-of-Function Mutations of c-KIT in Human Gastrointestinal Stromal Tumors, *Science* **1998**, *279*, 577-580.

[3] Kindblom, L. G.; Remotti, H. E.; Aldenborg, F.; Meis-Kindblom, J. M. Gastrointestinal Pacemaker Cell Tumor (Gipact): Gastrointestinal Stromal Tumors Show Phenotypic Characteristics of the Interstitial Cells of Cajal, *Am. J. Pathol.* **1998**, *152*, 1259-1269.

[4] Lennartsson, J.; Rönnstrand, L. Stem Cell Factor Receptor/C-Kit: From Basic Science to Clinical Implications, *Physiol. Rev.* **2012**, *92*, 1619-1649.

[5] Okada, S., Nakauchi, H., Nagayoshi, K., Nishikawa, S., Nishikawa, S., .; Miura, Y., .; Suda, T., Enrichment and Characterization of Murine Hematopoietic Stem Cells That Express C-Kit Molecule, *Blood* **1991**, *78*, 1706-1712.

[6] Oosterhuis, J. W.; Looijenga, L. H. J. Testicular Germ-Cell Tumors in a Broader Perspective, *Nature Reviews Cancer* **2005**, *5*, 210-222.

[7] Ray, P.; Krishnamoorthy, N.; Oriss, T. B.; Ray, A. Signaling of C-Kit in Dendritic Cells Influences Adaptive Immunity, *Ann. N. Y. Acad. Sci.* **2010**, *1183*, 104-122.

[8] Redegeld, F. A. In *Encyclopedia of Immunotoxicology*; Vohr, H.-W., Ed.; Springer Berlin Heidelberg: Berlin, Heidelberg, 2005, p 1-5.

[9] Wang, H.; Boussouar, A.; Mazelin, L.; Tauszig-Delamasure, S.; Sun, Y.; Goldschneider, D.; Paradisi, A.; Mehlen, P. The Proto-Oncogene C-Kit Inhibits Tumor Growth by Behaving as a Dependence Receptor, *Mol. Cell* **2018**, *72*, 413-425.

[10] Abbaspour Babaei, M.; Kamalidehghan, B.; Saleem, M.; Huri, H. Z.; Ahmadipour, F. Receptor Tyrosine Kinase (C-Kit) Inhibitors: A Potential Therapeutic Target in Cancer Cells, *Drug Des., Devel. Ther.* **2016**, *10*, 2443-2459.

[11] Joensuu, H.; Roberts, P. J.; Sarlomo-Rikala, M.; Andersson, L. C.; Tervahartiala, P.; Tuveson, D.; Silberman, S. L.; Capdeville, R.; Dimitrijevic, S.; Druker, B.; Demetri, G. D. Effect of the Tyrosine Kinase Inhibitor Sti571 in a Patient with a Metastatic Gastrointestinal Stromal Tumor, *N. Engl. J. Med.* **2001**, *344*, 1052-1056.

[12] Verweij, J.; Casali, P. G.; Zalcberg, J.; LeCesne, A.; Reichardt, P.; Blay, J.-Y.; Issels, R.; van Oosterom, A.; Hogendoorn, P. C. W.; Van Glabbeke, M.; Bertulli, R.; Judson, I. Progression-Free Survival in Gastrointestinal Stromal Tumours with High-Dose Imatinib: Randomised Trial, *The Lancet* **2004**, *364*, 1127-1134.

[13] Antonescu, C. R.; Besmer, P.; Guo, T.; Arkun, K.; Hom, G.; Koryotowski, B.; Leversha, M. A.; Jeffrey, P. D.; Desantis, D.; Singer, S. Acquired Resistance to Imatinib in Gastrointestinal Stromal Tumor Occurs through Secondary Gene Mutation, *Clin. Cancer Res.* **2005**, *11*, 4182-

4190.

[14] Dumez, H. Mechanisms of Resistance to Imatinib Mesylate in Gastrointestinal Stromal Tumors and Activity of the Pkc412 Inhibitor against Imatinib-Resistant Mutants, *Gastroenterology* **2005**, *128*, 270-279.

[15] Heinrich, M. C.; Corless, C. L.; Blanke, C. D.; Demetri, G. D.; Joensuu, H.; Roberts, P. J.; Eisenberg, B. L.; Mehren, M. V.; Fletcher, C. D. M.; Sandau, K. Molecular Correlates of Imatinib Resistance in Gastrointestinal Stromal Tumors, *J. Clin. Oncol.* **2006**, *24*, 4764.

[16] Gajiwala, K. S.; Wu, J. C.; Christensen, J.; Deshmukh, G. D.; Diehl, W.; Dinitto, J. P.; English, J. M.; Greig, M. J.; He, Y. A.; Jacques, S. L. Kit Kinase Mutants Show Unique Mechanisms of Drug Resistance to Imatinib and Sunitinib in Gastrointestinal Stromal Tumor Patients, *Proc. Nati. Acad. Sci. U. S. A.* **2009**, *106*, 1542-1547.

[17] George, S.; Wang, Q.; Heinrich, M. C.; Corless, C. L.; Zhu, M.; Butrynski, J. E.; Morgan, J. A.; Wagner, A. J.; Choy, E.; Tap, W. D.; Yap, J. T.; Abbeele, A. D. V. d.; Manola, J. B.; Solomon, S. M.; Fletcher, J. A.; Mehren, M. v.; Demetri, G. D. Efficacy and Safety of Regorafenib in Patients with Metastatic and/or Unresectable Gi Stromal Tumor after Failure of Imatinib and Sunitinib: A Multicenter Phase Ii Trial, *J. Clin. Oncol.* **2012**, *30*, 2401-2407.

[18] Garner, A. P.; Gozgit, J. M.; Anjum, R.; Vodala, S.; Schrock, A.; Zhou, T.; Serrano, C.; Eilers, G.; Zhu, M.; Ketzer, J.; Wardwell, S.; Ning, Y.; Song, Y.; Kohlmann, A.; Wang, F.; Clackson, T.; Heinrich, M. C.; Fletcher, J. A.; Bauer, S.; Rivera, V. M. Ponatinib Inhibits Polyclonal Drug-Resistant Kit Oncoproteins and Shows Therapeutic Potential in Heavily Pretreated Gastrointestinal Stromal Tumor (Gist) Patients, *Clin. Cancer Res.* **2014**.

[19] Lu, T.; Chen, C.; Wang, A.; Jiang, Z.; Qi, Z.; Hu, Z.; Hu, C.; Liu, F.; Wang, W.; Wu, H.; Wang, B.; Wang, L.; Qi, S.; Wu, J.; Wang, W.; Tang, J.; Yan, H.; Bai, M.; Liu, Q.; Liu, J.

Repurposing Cabozantinib to Gists: Overcoming Multiple Imatinib-Resistant Ckit Mutations Including Gatekeeper and Activation Loop Mutants in Gists Preclinical Models, *Cancer Letters* **2019**, *447*, 105-114.

[20] Gunnarsson, O.; Pfanzelter, N. R.; Cohen, R. B.; Keefe, S. M. Evaluating the Safety and Efficacy of Axitinib in the Treatment of Advanced Renal Cell Carcinoma, *Cancer Manag. Res.* **2015**, *7*, 65-73.

[21] Davis, M. I.; Hunt, J. P.; Herrgard, S.; Ciceri, P.; Wodicka, L. M.; Pallares, G.; Hocker, M.; Treiber, D. K.; Zarrinkar, P. P. Comprehensive Analysis of Kinase Inhibitor Selectivity, *Nat. Biotechnol.* **2011**, *29*, 1046.

[22] Zhou, W.; Ercan, D.; Chen, L.; Yun, C.-H.; Li, D.; Capelletti, M.; Cortot, A. B.; Chirieac, L.; Iacob, R. E.; Padera, R.; Engen, J. R.; Wong, K.-K.; Eck, M. J.; Gray, N. S.; Jänne, P. A. Novel Mutant-Selective Egfr Kinase Inhibitors against Egfr T790m, *Nature* **2009**, *462*, 1070.

[23] Liu, Y.; Gray, N. S. Rational Design of Inhibitors That Bind to Inactive Kinase Conformations, *Nat. Chem. Biol.* **2006**, *2*, 358.

[24] Zhao, Z.; Wu, H.; Wang, L.; Liu, Y.; Knapp, S.; Liu, Q.; Gray, N. S. Exploration of Type II Binding Mode: A Privilegedapproach for Kinase Inhibitor Focused Drug Discovery?, *ACS Chem. Biol.* **2014**, *9*, 1230-1241.

[25] Pemovska, T.; Johnson, E.; Kontro, M.; Repasky, G. A.; Chen, J.; Wells, P.; Cronin, C. N.; McTigue, M.; Kallioniemi, O.; Porkka, K.; Murray, B. W.; Wennerberg, K. Axitinib Effectively Inhibits Bcr-Abl1(T315I) with a Distinct Binding Conformation, *Nature* **2015**, *519*, 102.

[26] McTigue, M.; Murray, B. W.; Chen, J. H.; Deng, Y.-L.; Solowiej, J.; Kania, R. S. Molecular Conformations, Interactions, and Properties Associated with Drug Efficiency and Clinical Performance among VEGFR TK Inhibitors, *Proc. Nati. Acad. Sci. U. S. A.* **2012**, *109*, 18281-

18289.

[27] Gajiwala, K. S.; Wu, J. C.; Christensen, J.; Deshmukh, G. D.; Diehl, W.; DiNitto, J. P.; English, J. M.; Greig, M. J.; He, Y.-A.; Jacques, S. L.; Lunney, E. A.; McTigue, M.; Molina, D.; Quenzer, T.; Wells, P. A.; Yu, X.; Zhang, Y.; Zou, A.; Emmett, M. R.; Marshall, A. G.; Zhang, H.-M.; Demetri, G. D. Kit Kinase Mutants Show Unique Mechanisms of Drug Resistance to Imatinib and Sunitinib in Gastrointestinal Stromal Tumor Patients, *Proc. Nati. Acad. Sci. U. S. A.* **2009**, *106*, 1542-1547.

[28] Kissova, M.; Maga, G.; Crespan, E. The Human Tyrosine Kinase Kit and Its Gatekeeper Mutant T670i, Show Different Kinetic Properties: Implications for Drug Design, *Bioorg. Med. Chem.* **2016**, *24*, 4555-4562.

Table of Contents Graphic